Physical-layer Security of Uplink mmWave Transmissions in Cellular V2X Networks

Tong-Xing Zheng, *Member, IEEE*, Yating Wen, Hao-Wen Liu, Ying Ju, *Member, IEEE*, Hui-Ming Wang, *Senior Member, IEEE*, Kai-Kit Wong, *Fellow, IEEE*, and Jinhong Yuan, *Fellow, IEEE*

***Abstract*—In this paper, we investigate physical-layer security of the uplink millimeter wave communications for a cellular vehicle-to-everything (C-V2X) network comprised of a large number of base stations (BSs) and different categories of V2X nodes, including vehicles, pedestrians, and road side units. Considering the dynamic change and randomness of the topology of the C-V2X network, we model the roadways, the V2X nodes on each roadway, and the BSs by a Poisson line process, a 1D Poisson point process (PPP), and a 2D PPP, respectively. We propose two uplink association schemes for a typical vehicle, namely, the smallest-distance association (SDA) scheme and the largest-power association (LPA) scheme, and we establish a tractable analytical framework to comprehensively assess the security performance of the uplink transmission, by leveraging the stochastic geometry theory. Specifically, for each association scheme, we first obtain new expressions for the association probability of the typical vehicle, and then derive the overall connection outage probability and secrecy outage probability by calculating the Laplace transform of the aggregate interference power. Numerical results are presented to validate our theoretical analysis, and we also provide interesting insights into how the security performance is influenced by various system parameters, including the densities of V2X nodes and BSs. Moreover, we show that the LPA scheme outperforms the SDA scheme in terms of secrecy throughput.**

***Index Terms*—Cellular vehicle-to-everything, physical-layer security, millimeter wave, stochastic geometry, Poisson line process, Poisson point process**

Manuscript received XX XX, 2021; revised XX XX, 20XX; accepted XX XX, 2022. Date of publication XX XX, 2022; date of current version XX XX, 2022. The work of T.-X. Zheng, Y. Wen, and H.-W. Liu was supported in part by the National Natural Science Foundation of China under Grant 61701390, in part by the Open Research Fund of National Mobile Communications Research Laboratory, Southeast University, under Grant 2021D07, in part by the China Postdoctoral Science Foundation under Grants 2021M702631, in part by the Natural Science Basic Research Plan of Shaanxi Province under Grant 2022JM-320, and in part by the Fundamental Research Funds for the Central Universities under Grant xzy012021033. The work of Y. Ju was supported in part by the National Natural Science Foundation of China under Grant 62102301, and in part by the Guangdong Basic and Applied Basic Research Foundation under Grant 2020A1515110772. The work of H.-M. Wang was supported in part by the National Natural Science Foundation of China under Grants 61941105 and 62171364. The work of K.-K. Wong was supported in part by the Engineering and Physical Sciences Research Council under Grant EP/T015985/1. The work of J. Yuan was supported in part by the Australia Research Council Discovery Project under Grant DP220103596 and Linkage Project under Grant LP200301482. The associate editor coordinating the review of this paper and approving it for publication was P. Li. *(Corresponding author: Tong-Xing Zheng.)*

T.-X. Zheng, Y. Wen, H.-W. Liu, and H.-M. Wang are with the Faculty of Electronic and Information Engineering, Xi'an Jiaotong University, Xi'an 710049, China. T.-X. Zheng is also with the National Mobile Communications Research Laboratory, Southeast University, Nanjing 210096, China. T.-X. Zheng and H.-M. Wang are also with the Ministry of Education Key Laboratory for Intelligent Networks and Network Security, Xi'an Jiaotong University, Xi'an 710049, China (e-mail: zhengtx@mail.xjtu.edu.cn, wyt461246@stu.xjtu.edu.c, hwliu.xjtu@gmail.com, xjbswhm@163.com).

Y. Ju is with the Department of Telecommunications Engineering, Xidian University, Xi'an 710071, China, and also with the State Key Laboratory of Integrated Services Networks, Xidian University, Xi'an 710071, China (e-mail: juyingtju@163.com).

K.-K. Wong is with the Department of Electronic and Electrical Engineering, University College London, WC1E 6BT London, U.K. (e-mail: kai-kit.wong@ucl.ac.uk).

J. Yuan is with the School of Electrical Engineering and Telecommunications, University of New South Wales, Sydney, NSW 2052, Australia (e-mail: j.yuan@unsw.edu.au).

I. Introduction

Cellular vehicle-to-everything (C-V2X), which enables vehicles to exchange information in real-time with other vehicles (V2V), pedestrians (V2P), infrastructures (V2I), and even base stations (V2B), plays a significant role in guaranteeing traffic efficiency, road safety, and transport reliability, and has been envisioned as a core technology for catalyzing a much smarter and safer vehicular communication network [1]–[4]. In fact, various V2X standards have been launched worldwide to enhance the interoperability of communications between vehicles during the past decades, e.g., the dedicated short-range communications [5], the intelligent transportation system (ITS) [5], [6], the wireless access for vehicular environment (WAVE) [7], the communication access for land mobiles [5], etc. However, the majority of earlier V2X standards are based on IEEE 812.11p technology which suffers from unbounded channel access delay and lack of quality of service guarantee, since it is originally devised for the wireless local area network with low mobility [5], [6]. Recently, the 3rd Generation Partnership Project has started exploring the combination of V2X networks and cellular networks [7], [8] to meet demanding requirements of V2X services with high mobility. With the forthcoming beyond 5G and 6G era, the tremendous data traffic places an unprecedented demand on ultra-high capacity and ultra-low latency for C-V2X networks. To overcome this challenge, millimeter wave (mmWave) communication is expected to be an effective solution for increasing the capacity and reducing latency owing to its large available spectrum resources and small data packets [9], [10]. Meanwhile, by generating highly directional beamforming via mmWave antenna arrays, the Doppler spread effect at high speeds can be significantly mitigated [11].

Besides capacity and latency, information security should be a primary concern when designing C-V2X networks. For example, once some confidential information of vehicular communications is leaked to malicious attackers, traffic accidents might be induced by various attacks, resulting in significant loss of property and even endangering human lives. Key based

cryptographic encryption is a common and effective method to safeguard communication security [12], which however will encounter several difficulties when being implemented in C-V2X networks, e.g., being comprised when the attackers possess inexhaustible computing power, being impractical due to the costly large-scale key storage, management, and distribution, and causing intolerable latency due to complicated cryptographic algorithms. Against this background, physical-layer security (PLS) [13]–[17] can be leveraged as a powerful complementary solution to protect wireless security for C-V2X networks. PLS is an information-theoretic approach which achieves secure wireless transmission by exploiting the randomness of noise and the characteristics of wireless channels, and has been extensively investigated as a low-complexity security method for wireless communications. In view of the above discussion, in this paper, we aim to explore the potential of PLS for realizing a secure mmWave C-V2X network.

A. Previous Works

Early works on vehicular networks have mainly focused on the performance analysis of system-level simulations, which are often time-consuming, and more importantly cannot reveal the impacts of system parameters on the network performance. During recent years, the stochastic geometry theory has been introduced to ease the theoretical analysis for vehicular networks, with which it is much more convenient to provide tractable analytical expressions [18]–[24]. For the V2X networks, the roadways are generally predominantly straight but randomly oriented and the locations of the V2X nodes, including vehicles, pedestrians, and road side units (RSUs), on each road are often irregular. In order to characterize the irregularity and randomness of the V2X networks, a canonical spatial model, namely, Cox process or doubly stochastic Poisson point process (PPP), has been widely adopted with which the roads in the network are modeled by a Poisson line process (PLP) and the locations of the V2X nodes on each road are modeled by a 1D homogeneous PPP [20], [22]. By doing this, the locations of transmitting and receiving nodes can be characterized by two Cox processes driven by the same PLP. Moreover, when it comes to C-V2X networks, the locations of base stations (BSs) and users can be modeled by homogeneous 2D PPPs [21], [24]. Based on the above stochastic geometry models, analytically tractable results, in terms of interference distribution, association probability, coverage and rate can be expediently derived [20]–[24].

In recent years, the performance analysis of mmWave vehicular networks has captured a stream of research [25]–[29]. For instance, the coverage performance was analyzed for mmWave V2V networks [26], V2X networks [27], and C-V2I networks [28], considering either a single street or multiple cross streets. *Yi et al.* [29] investigated the coverage probability of an mmWave vehicular platoon system on a multi-lane road, considering both the blockage caused by vehicles and distinguished line-of-sight (LOS) and non-line-of-sight (NLOS) transmissions. However, the above works have only focused on mmWave V2X networks with quite simple spatial models for roads and have ignored the random directivity of multiple roads.

PLS has not been studied in cellular vehicular networks until recently [30]–[33]. *Ahn et al.* [30] derived the secrecy capacity of PLS for vehicular networks. *Ai et al.* [31] analyzed the average secrecy capacity for V2V communications under a double Rayleigh fading channels and considered the impacts of fading, path loss, and eavesdropper location. *Wang et al.* [32] established an analysis framework to explore the optimal secrecy throughput of a V2V network based on a maximum SIN association scheme. *Wang et al.* further investigated the potential of AN techniques in safeguarding security for C-V2X networks in [33]. Note that all these works have focused on the PLS in the microwave vehicular networks rather than in the mmWave ones.

So far, the PLS in the mmWave vehicular networks has only been investigated in [34], where the authors considered an mmWave V2V network consisting of a pair of legitimate transmitter and receiver against an eavesdropper, and they designed both analog beamforming and hybrid analog/digital precoders with AN injection for improving the secrecy rate.

B. Our Work and Contributions

Inspired by the aforementioned endeavors, we for the first time explore the PLS of uplink mmWave communications in C-V2X networks under a stochastic geometry framework, considering various random resources, including small-scale channel fading, large-scale path loss, blockage effect, LOS and NLOS links, as well as network topology and node distribution. The main contributions of our work are summarized as follows:

- We build a comprehensive and tractable mathematical framework for analyzing the secrecy and reliability performance for an mmWave C-V2X network from the stochastic geometry theory, where we model the roadways, the V2X nodes on each roadway, and the BSs by a PLP, a 1D Poisson point process (PPP), and a 2D PPP, respectively.
- We propose two uplink association schemes to connect a typical transmitting vehicle to either a V2X node (e.g., a vehicle, a pedestrian, or a RSU) or a BS, namely, the smallest-distance association (SDA) scheme and the largest-power association (LPA) scheme, respectively. Under each scheme, we derive the distribution of the distance between the typical vehicle and its intended receiver, based on which we calculate the corresponding association probability.
- Focusing on either the V2X or V2B communication in each association scheme, we derive exact analytical expressions for both the connection outage probability (COP) and secrecy outage probability (SOP), which are expressed in terms of the Laplace transform of the aggregate interference power in the network. Furthermore, we characterize the trade-off between transmission reliability and secrecy by evaluating the secrecy throughput.
- We present various numerical results to validate our theoretical analyses and uncover the impacts of key

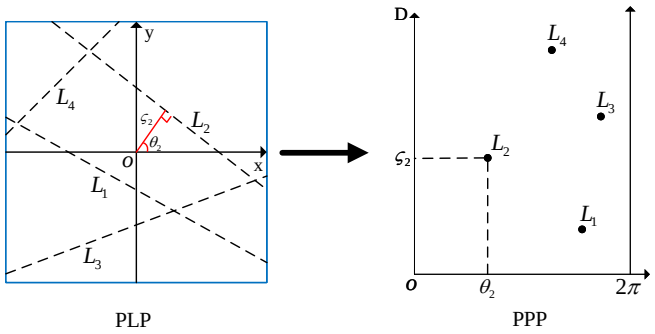

Fig. 1. Illustration of mapping from a PLP on the 2D plane $\mathbb{R}^2$ (left) to a PPP on the representation space $\mathcal{C}$ (right), e.g., line L_2 on $\mathbb{R}^2$ is mapped to a point on $\mathcal{C}$ with coordinates (ζ_2, θ_2).

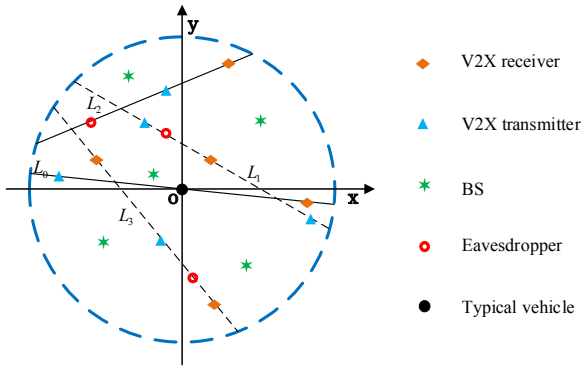

Fig. 2. A snapshot illustration of a C-V2X network. The typical vehicle at the origin communicates to either a V2X receiver on a road or a BS, and the ongoing message delivery is potentially wiretapped by the eavesdroppers.

system parameters, including the densities of V2X nodes and BSs, on the transmission reliability and secrecy performance for both the SDA and LPA schemes. We show that the LPA scheme outperforms the SDA one in terms of secrecy throughput.

C. Organization and Notations

The rest of this paper is organized as follows. The mathematical preliminary for Poisson line process is given in Section II. The system model and problem description are presented in Section III. In Section V, the COP and SOP of the uplink mmWave transmission are derived. Numerical results are provided in Section VI. Conclusions are drawn in Section VII.

Notations: $\mathbb{P}[\cdot]$ denotes the probability operator. $\mathbb{E}_X[f(X)]$ denotes the expectation of the function $f(X)$ taken over a random variable X. $\mathcal{L}_X(s) \triangleq \mathbb{E}_X\left[e^{-sX}\right]$ denotes the Laplace transform of X at s. $\mathbf{I}_n(\cdot)$ for $n = 0, 1$ and $\mathbf{L}_n(\cdot)$ for $n = 1, 0, -1$ denote the modified Bessel function of the first kind and the modified Struve function, respectively [40].

II. Mathematical Preliminary: Poisson Line Process

Since the PLP will be employed to model the distribution of roads in the C-V2X network under investigation, the concept of PLP and its properties are briefly introduced in this section, while a thorough knowledge of the PLP theory can be found in [20], [22], [39].

Definition 1 (Poisson line process): For the Cartesian coordinates, an arbitrary undirected line L_k on the 2D plane $\mathbb{R}^2$ can be uniquely characterized by its perpendicular distance $\zeta_k \in \mathbb{R}^+$ from the origin $o(0,0)$ and the angle $\theta_k \in [0, 2\pi)$ between the perpendicular line from the origin and the positive x-axis. The parameter pair (ζ_k, θ_k) can be interpreted as the coordinates of a point on the 2D cylindrical surface $\mathcal{C} \equiv \mathbb{R}^+ \times [0, 2\pi)$, which is termed the representation space. This indicates a one-to-one mapping between the lines on the 2D plane $\mathbb{R}^2$ and the points on the representation space $\mathcal{C}$, as illustrated in Fig. 1. Then, a PLP can be defined as a random collection of lines on $\mathbb{R}^2$, which are constructed from a set of points generated by a PPP on $\mathcal{C}$.

Definition 2 (Stationarity and motion-invariance): A line process $\Phi_L = \{L_1, L_2, \cdots\}$ on $\mathbb{R}^2$ is deemed to be stationary if a translated line process $T(\Phi_L) = \{T(L_1), T(L_2), \cdots\}$ shares the same distribution as Φ_L for any translation T on $\mathbb{R}^2$. Similarly, Φ_L is motion-invariant if the distribution of lines remains invariant when rotating the axes with an arbitrary angle θ on $\mathbb{R}^2$.

For analytical simplicity, we assume that the PLP is stationary and motion-invariant.

Definition 3 (Line density): The line density λ_L of a PLP Φ_L is defined as the average line length per unit area. If Φ_L is a motion-invariant line process, the density μ_L of the corresponding point process on the representation space $\mathcal{C}$ can be given by $\mu_L = \lambda_L / \pi$.

III. System Model

This paper considers an mmWave C-V2X network consisting of multiple irregularly oriented roads with vehicles, pedestrians, and road side units (RSUs) randomly distributed on them, coexisting with BSs stochastically deployed in the network, as illustrated in Fig. 2. For convenience, all the vehicles, pedestrians, and RSUs are collectively called V2X nodes. We aim to investigate the uplink secure communication of an arbitrary vehicle which transmits confidential messages to either a V2X node or a BS following certain association policies in the presence of untrusted V2X nodes (eavesdroppers) potentially overhearing the over-the-air secrecy transmission.

A. Network Model

Since the locations of vehicles, pedestrians, and RSUs are restricted to roads, we first model the spatial distribution of the roads by a stationary and motion-invariant PLP Φ_L with line density λ_L [21]–[24]. The density of the equivalent PPP of Φ_L on the representation space $\mathcal{C}$ is given by $\mu_L = \lambda_L / \pi$. We model the locations of vehicles, pedestrians, and RSUs on the k-th line $L_k \in \Phi_L$ by independent and homogeneous 1D PPPs $\Omega_{L_k}^{(v)}$, $\Omega_{L_k}^{(p)}$, and $\Omega_{L_k}^{(r)}$ with densities μ_v, μ_p, and μ_r, respectively. We also model the locations of BSs by a homogeneous 2D PPP Φ_B with density λ_B. Hence, the density of V2X nodes on an arbitrary line is $\mu = \mu_v + \mu_p + \mu_r$.

Assuming that each V2X node transmits with a probability p_t, the locations of V2X transmitters on the k-th road can be modeled as a thinned 1D PPP $\Omega_{L_k}^T$ with density $\mu^T = p_t\mu$. We also assume that the vehicle and pedestrian receivers have a probability p_e of being untrusted which passively wiretap the uplink secure transmission from the vehicle transmitters. The locations of the potential eavesdroppers on the k-th road can be modeled as a thinned 1D PPP $\Omega_{L_k}^E$ with density $\mu^E = p_e\left(1-p_t\right)\left(\mu_v+\mu_p\right)$. Therefore, the locations of the trusted V2X receivers can be modeled as a thinned 1D PPP $\Omega_{L_k}^R$ with density $\mu^R = \left(1-p_t\right)\left(\mu_r+\left(1-p_e\right)\left(\mu_p+\mu_v\right)\right)$.[1]

In order to explore the uplink secure communication performance of an arbitrary vehicle in the C-V2X network, we focus on a typical vehicle which is placed at the origin of coordinates as shown in Fig. 2. Specifically, we add a line through the origin as a typical line, denoted as L_0, such that a new PLP $\Phi_{L_0} \triangleq \Phi_L \cup L_0$ is formed which shares the same distribution with the original PLP Φ_L.[2] Besides, the locations of the V2X nodes on L_0 are modeled as the same 1D homogeneous PPP as other lines. We then place a vehicle of interest at the origin as the typical vehicle, which does not change the distribution of other nodes in the network but will significantly ease the performance analysis from a network-wide perspective. As a consequence, the location sets of V2X transmitters and receivers in the network can be represented by $\Xi^T = \{\Omega_{L_k}^T\}_{L_k\in\Phi_{L_0}}$ and $\Xi^R = \{\Omega_{L_k}^R\}_{L_k\in\Phi_{L_0}}$, respectively. Key notations are summarized in Table I. Throughout this paper, we use notations Φ and Ω to differentiate the 2D and 1D Poisson processes.

B. MmWave Communication Model

This subsection details the model of mmWave communications with special characteristics.

1) Directional Beamforming: To overcome the severe path loss, all the nodes in the network, including V2X nodes and BSs, are equipped with highly directional antenna arrays. The gain pattern of the antenna array is described by the following sectored model [14], [35], [36],

$$G_\tau\left(\eta\right) = \begin{cases} M_\tau, & |\eta| \le \eta_\tau \\ m_\tau, & otherwise \end{cases} \tag{1}$$

where $\tau \in \{z, b\}$[3] denotes the type of nodes in the network, i.e., V2X nodes or BSs, $\eta \in [-\pi, \pi)$ is the angle of the boresight direction, η_τ is the half beam width of the main lobe, and M_τ and m_τ denote the array gains of the main and side lobes, respectively.

For simplicity, we assume that the antenna beams of the desired link are aligned. Hence, we express the gain for a desired link as $G_{x,y} = M_xM_y$, where x and y denote the locations of transmitter and receiver, respectively. The antenna gains for the other links depend on their respective directivity gains of the main and side lobes, which can be described as [35], [37]

$$G_{x,y} = \begin{cases} M_xM_y, & \Pr_{M_xM_y} = \dfrac{\eta_x\eta_y}{\pi^2} \\ M_xm_y, & \Pr_{M_xm_y} = \dfrac{\eta_x\left(\pi-\eta_y\right)}{\pi^2} \\ m_xM_y, & \Pr_{m_xM_y} = \dfrac{\left(\pi-\eta_x\right)\eta_y}{\pi^2} \\ m_xm_y, & \Pr_{m_xm_y} = \dfrac{\left(\pi-\eta_x\right)\left(\pi-\eta_y\right)}{\pi^2} \end{cases} \tag{2}$$

where η_x and η_y respectively represent the half beam width of the main lobe for transmitter and receiver, and $\Pr_{G_{x,y}}$ denotes the probability of having a specific antenna gain $G_{x,y}$.

2) Blockage Model: Since mmWave communications are sensitive to blockage, the LOS and NLOS links have different transmission characteristics [14], [35]–[37]. Using the model proposed in [14], we define $q_{\mathrm{L}}\left(r\right) = e^{-\beta r}$ and $q_{\mathrm{N}}\left(r\right) = 1 - q_{\mathrm{L}}\left(r\right)$ as the probability that a link at distance r is LOS and NLOS, respectively, where r and β denote the distance between the transmitter and receiver and the density of blockage, respectively.[4]

3) Path Loss: The path loss for a link between nodes x and y can be expressed as $r_{x,y}^{-\alpha_j}$, for $j \in \{\mathrm{L}, \mathrm{N}\}$, where $r_{x,y}$ denotes the distance, α_{L} and α_{N} denote the path-loss exponents for the LOS and NLOS links, respectively [35], [36]. Besides, we adopt a slight abuse of α in some equations, e.g., (25)–(27), and one can easily differentiate the two cases from the context.

4) Small-Scale Fading: We focus on the scenario of slow fading channels and adopt a generic assumption that the mmWave wireless channels undergo independent Nakagami-m fading, where the fading parameters for LOS and NLOS links are denoted as positive integers m_{L} and m_{N}, respectively [10], [14]. Note that $m_j = 1$ corresponds to Rayleigh fading whereas a large m_j can be used to approximate the small-variance fading such as the LOS case. Following Nakagami-m fading, the channel gain $|h_{x,y}|^2$ from x to y can be modeled as a normalized Gamma random variable, i.e., $|h_{x,y}|^2 \sim \Gamma\left(m_j, 1/m_j\right)$ for $j \in \{\mathrm{L}, \mathrm{N}\}$.

C. User Association Scheme

In this subsection, we propose two association schemes for the uplink transmission from the typical vehicle to a V2X receiver or a BS, namely, the smallest-distance association (SDA) scheme and the largest-power association (LPA) scheme. Specifically, in the SDA scheme, the typical vehicle is associated with the nearest receiver; while in the LPA scheme, the typical vehicle accesses to the receiver who has the largest average received power. In general, the SDA scheme is equivalent to the LPA scheme in the microwave uplink communication. However, due to the remarkable impacts of the LOS and NLOS links in mmWave transmission, a receiver with NLOS link status may have a small average received

[1]Throughout the paper, the untrusted and trusted V2X receivers are called eavesdroppers and V2X receivers, respectively.

[2]The Slivnyak's theorem in [38] implies that the addition or removal of a line or a node in a vehicular network does not change the distribution of other lines or nodes.

[3]It is worth noting that, z and b are used to denote the locations of a V2X node and a BS, respectively. Assuming that all the V2X nodes share the same system parameters, we adopt a slight misuse and let z and b denote different types of nodes.

[4]Throughput this paper, we use the subscripts L and N to differentiate LOS and NLOS links.

TABLE I
SUMMARY OF KEY NOTATIONS

Symbol	Definition
Φ_L, Φ_{L_0}	PLPs of roads except the typical line and of all roads
λ_L, μ_L	Densities of roads on the 2D plane and of the equivalent points on the representation space
$\Omega_{L_k}^{(v)}$, $\Omega_{L_k}^{(p)}$, $\Omega_{L_k}^{(r)}$	PPPs of vehicles, pedestrians, and RSUs on the k-th line
μ_v, μ_p, μ_r	Densities of vehicles, pedestrians, and RSUs on an arbitrary line
$\Omega_{L_k}^{T}$, $\Omega_{L_k}^{R}$, $\Omega_{L_k}^{E}$	PPPs of V2X transmitters, V2X receivers, and eavesdroppers on the k-th line
μ^T, μ^R, μ^E	Densities of V2X transmitters, V2X receivers, and eavesdroppers on an arbitrary line
Ξ^T, Ξ^R	PPPs of V2X transmitters and V2X receivers on the 2D plane
p_t, p_e	Probabilities of a V2X node transmitting and eavesdropping
Φ_B, λ_B	PPP of BSs and its density
α_{L}, α_{N}	Path-loss exponents of LOS and NLOS links

power compared with a closer receiver with LOS link status. In reality, the switch of users in 5G New Radio (NR) system relies on the channel state information, and the switch decision can be controlled by gNB or themselves. In this study, the LPA scheme can match well with the real switch strategy in 5G NR, and the SDA scheme can be regarded as an alternative scheme with a low complexity. In addition, we assume the typical vehicle can work well with PC5 interface and Uu interface, i.e., the typical vehicle can transmit the real-time information to an arbitrary BS or a V2X receiver.

It is worthy noting that, we mainly use the large-scale path loss, which dominates the signal attenuation for mmWave, to determine the association criterion, while ignoring the small-scale channel fading. This makes the proposed association schemes efficient and easy-to-implement. Besides, our association schemes can fully reflect the characteristics of the geometry of the mmWave C-V2X networks by incorporating the random network topology of the C-V2X networks and the coexistence feature of LOS and NLOS links for mmWave communications.

Whatever association scheme is chosen, the transmitting V2X nodes and BSs other than the typical vehicle are deemed to be the interference nodes, and all the eavesdroppers always passively listen to the ongoing secure transmission from the typical vehicle.

D. Performance Metrics

For the sake of secure wireless transmission, we adopt the well-known Wyner's wiretap encoding scheme to encode classified messages before transmission [13]. We denote the codeword rate and secrecy rate as R_t and R_s, respectively. The rate redundancy $R_e \triangleq R_t - R_s$ is exploited to provide secrecy against eavesdropping. Due to channel fading and lack of global channel state information, perfect reliability and secrecy cannot always be guaranteed with target code rates. In addition, for slow fading channels where the channel coherence time is much longer than the symbol duration, it is more appropriate to use the outage-based metrics with fixed rates to measure communication performance, instead of using ergodic-based metrics requiring encoding over a large number of channel states, since the latter will cause an unacceptably large delay. Hence, we adopt the following outage-based metrics to measure transmission reliability and secrecy from a probabilistic perspective.

- **Connection Outage Probability**: If the legitimate channel capacity C_t exceeds R_t, the codewords can be decoded by the desired receiver. Otherwise, a connection outage event occurs, and the corresponding probability is called the COP, which is denoted as $\mathcal{P}_{co}$ [36].
- **Secrecy Outage Probability**: If the wiretap channel capacity C_e is larger than R_e, perfect secrecy cannot be safeguarded, and then a secrecy outage event happens. The probability of the secrecy outage event is referred to as the SOP, which is denoted as $\mathcal{P}_{so}$ [36].
- **Secrecy Throughput**: Secrecy throughput quantifies the average effectively conveyed information bits per second per Hertz subject to an SOP constraint and is formulated as

$$\Psi = (1 - \mathcal{P}_{co})\, R_s, \quad \text{s.t.} \quad \mathcal{P}_{so} \leq \epsilon, \tag{3}$$

  where $\epsilon \in [0, 1]$ denotes the SOP threshold, i.e., the maximum tolerable SOP.

In the following, we will first investigate the association probabilities for different association schemes. Subsequently, we will derive the COP and SOP of the secure uplink transmission under each association scheme, which finally yields the secrecy throughput.

IV. ASSOCIATION PROBABILITIES

In this section, to facilitate the COP and SOP analysis on the PLS for an mmWave C-V2X network, we first examine the statistics of the distance between the typical vehicle and the associated receiver for two association schemes, namely, SDA and LPA schemes, and derive association probabilities for both schemes.

A. Association Probabilities for SDA Scheme

In the SDA scheme, the distribution of the distance between the typical vehicle and its associated receiver and their corresponding association probabilities are detailed in the following.

Lemma 1: The cumulative distribution function (CDF) and probability density function (PDF) of the distance $r_{o,z}$ between the typical vehicle and the nearest V2X receiver located at z are respectively given by

$$F_z\left(r_{o,z}\right) = 1 - \exp\Bigg(- 2\pi\mu^R r_{o,z} - 4\pi\mu_L r_{o,z} - \pi^2\mu_L r_{o,z}\Big[\mathbf{L}_1\left(2\mu^R r_{o,z}\right) - I_1\left(2\mu^R r_{o,z}\right)\Big]\Bigg), \quad (4)$$

$$f_z\left(r_{o,z}\right) = 2\mu^R\Bigg(\pi^2\mu_L\Big[I_0\left(2\mu^R r_{o,z}\right) - \mathbf{L}_0\left(2\mu^R r_{o,z}\right)\Big] + 1\Bigg)\times \exp\Bigg(- 2\pi\mu_L r_{o,z} + \pi^2\mu_L r_{o,z}\Big[\mathbf{L}_{-1}\left(2\mu^R r_{o,z}\right) - I_1\left(2\mu^R r_{o,z}\right)\Big] - 2\mu^R r_{o,z}\Bigg). \quad (5)$$

Proof: The results directly follow from [24, Lemma 1]. ∎

Lemma 2: The CDF and PDF of the distance $r_{o,b}$ between the typical vehicle and the nearest BS located at b are respectively expressed as

$$F_b\left(r_{o,b}\right) = 1 - e^{-\pi\lambda_B r_{o,b}^2}, \quad (6)$$

$$f_b\left(r_{o,b}\right) = 2\pi\lambda_B r_{o,b} e^{-\pi\lambda_B r_{o,b}^2}. \quad (7)$$

Proof: The results directly follow from the void probability of a PPP [38], [39]. ∎

It can be observed that the distribution of $r_{o,z}$ in Lemma 1 is much more complicated than that of $r_{o,b}$ in Lemma 2. The fundamental reason is that the distribution of V2X nodes follows a complex Cox process or doubly stochastic PPP while that of BSs simply obeys a homogeneous PPP. Using the above lemmas, the probabilities of associating the typical vehicle to a V2X node (V2X link) and to a BS (V2B link) can be calculated by the following theorem.

Theorem 1: In the SDA scheme, the association probabilities of V2X and V2B links are respectively given by

$$\mathcal{P}_{v2x}^{\mathrm{SDA}} = \int_0^\infty F_z\left(r_{o,b}\right) f_b\left(r_{o,b}\right) dr_{o,b}, \quad (8)$$

$$\mathcal{P}_{v2b}^{\mathrm{SDA}} = 1 - \mathcal{P}_{v2x}^{\mathrm{SDA}}, \quad (9)$$

where $F_z\left(r_{o,z}\right)$ and $f_b\left(r_{o,b}\right)$ are given in (4) and (7), respectively.

Proof: Conditioned on a given distance $r_{o,b}^*$ between the typical vehicle and the nearest BS, the association probability of the V2X link for the SDA scheme can be described as

$$\mathcal{P}_{v2x}^{\mathrm{SDA}}\left(v2x|\, r_{o,b}^*\right) = \mathbb{P}\left[r_{o,z}^* \le r_{o,b}^* \middle|\, r_{o,b}^*\right], \quad (10)$$

where $r_{o,z}^*$ denotes the distance between the typical vehicle and the nearest V2X receiver.

Using the CDF of $r_{o,z}^*$ in (4), (10) can be rewritten as

$$\mathcal{P}_{v2x}^{\mathrm{SDA}}\left(v2x|\, r_{o,b}^*\right) = F_z\left(r_{o,b}^*\right). \quad (11)$$

Hence, the association probability of a V2X link for the SDA scheme can be calculated as

$$\mathcal{P}_{v2x}^{\mathrm{SDA}} = \mathbb{E}_{r_{o,b}^*}\left[\mathcal{P}_{v2x}^{\mathrm{SDA}}\left(v2x|\, r_{o,b}^*\right)\right] = \int_0^\infty F_z\left(r_{o,b}\right) f_b\left(r_{o,b}\right) dr_{o,b}. \quad (12)$$

It is obvious that the association probability of the V2B link $\mathcal{P}_{v2b}^{\mathrm{SDA}}$ is the complementary probability to $\mathcal{P}_{v2x}^{\mathrm{SDA}}$. ∎

B. Association Probabilities for LPA Scheme

Revisiting the LPA scheme, if the typical vehicle is associated with a V2X node, it is not difficult to express the location of the best V2X receiver z^* as below

$$z^* = \arg\max_{z\in\Xi^R} P_t G_{o,z} r_{o,z}^{-\alpha} = \arg\min_{z\in\Xi^R} \frac{r_{o,z}^\alpha}{P_t G_{o,z}} = \arg\min_{L_k\in\Phi_{L_0}} \min_{z\in\Omega_{L_k}^R} \frac{r_{o,z}^\alpha}{P_t G_{o,z}}. \quad (13)$$

where P_t denotes the transmit power of a V2X transmitter.

The above result indicates that, the target receiver should have the minimal $r_{o,z}^\alpha/\left(P_t G_{o,z}\right)$ than any others on the same roads, and then we should select the one with the minimum $r_{o,z}^\alpha/\left(P_t G_{o,z}\right)$ of all the roads as the target receiver. Specifically, consider a 1D PPP $\Omega_{L_k}^R$ for the V2X receivers on the k-th line, the coordinate of which is denoted as (ζ_k, θ_k) in the cylindrical surface, and we transform $\Omega_{L_k}^R$ to a new 1D PPP Ω_k leveraging the Mapping Theorem of a PPP [39] with mapping function $r_{o,z}^\alpha/\left(P_t G_{o,z}\right)$, i.e.,

$$\Omega_k = \left\{\rho \triangleq \frac{r_{o,z}^\alpha}{P_t G_{o,z}}, z \in \Omega_{L_k}^R, r_{o,z} = \sqrt{\zeta_z^2 + \zeta_k^2}, \right\}, \quad (14)$$

where $z \in \Omega_{L_k}^R$ is the location of the randomly distributed V2X receiver, ζ_z is the distance between the receiver at z and the intersection of the k-th line and its perpendicular line passing through the origin.

Obviously, the candidate receiver in Ω_k must have the smallest ρ, i.e., the candidate is closest to the origin. Hence, instead of deriving the location distribution of the target receiver location, we can simply examine the distribution of its distance in the mapping domain. For convenience, we define $\Omega_k^{\mathrm{1D}} \triangleq \left\{\Omega_k\right\}_{L_k\in\Phi_{L_0}}$ as the union process of the mapped PPP. Based on the above analysis, we derive the CDF and PDF of the shortest distance ρ in the following.

Lemma 3: The CDF of the shortest distance ρ in the mapped PPP Ω_k^{1D} is given by

$$F_\rho\left(\rho\right) = 1 - \exp\Bigg(- \Lambda_0\big[0,\rho\big] - 2\pi\mu_L\int_0^D\Big[1 - \exp\left(-\Lambda_{\zeta_k}\left[0,\rho\right]\right)\Big]d\zeta_k\Bigg), \quad (15)$$

where

$$\Lambda_{\zeta_k}\left[0,\rho\right] = \int_0^{\sqrt{\left(P_t G_{o,z}\rho\right)^{\frac{2}{\alpha_{\mathrm{L}}}} - \zeta_k^2}} 2\mu^R e^{-\beta\sqrt{\zeta_k^2+\zeta_z^2}} d\zeta_z + \int_0^{\sqrt{\left(P_t G_{o,z}\rho\right)^{\frac{2}{\alpha_{\mathrm{N}}}} - \zeta_k^2}} 2\mu^R\left(1 - e^{-\beta\sqrt{\zeta_k^2+\zeta_z^2}}\right) d\zeta_z, \quad (16)$$

and $\Lambda_0\left[0,\rho\right]$ is the result of (16) with $\zeta_k = 0$.

Proof: The proof is given in Appendix A. ∎

Corollary 1: The PDF of the shortest distance ρ in the mapped PPP Ω_k^{1D} is given by

$$f_\rho(\rho) = \exp\left(-\Lambda_0[0,\rho] - 2\pi\mu_L \int_0^D \left[1 - e^{-\Lambda_{\zeta_k}[0,\rho]}\right] d\zeta_k\right) \times \left[\frac{d\Lambda_0[0,\rho]}{d\rho} + 2\pi\mu_L \int_0^D e^{-\Lambda_{\zeta_k}[0,\rho]} \frac{d\Lambda_{\zeta_k}[0,\rho]}{d\rho} d\zeta_k\right], \quad (17)$$

where

$$\frac{d\Lambda_{\zeta_k}[0,\rho]}{d\rho} = 2\mu^R e^{-\beta(P_t G_{o,z}\rho)^{\frac{1}{\alpha_{\mathrm{L}}}}} \frac{P_t G_{o,z}(P_t G_{o,z}\rho)^{\frac{2}{\alpha_{\mathrm{L}}}-1}}{\alpha_{\mathrm{L}}\sqrt{(P_t G_{o,z}\rho)^{\frac{2}{\alpha_{\mathrm{L}}}} - \zeta_k^2}} + 2\mu^R\left(1 - e^{-\beta(P_t G_{o,z}\rho)^{\frac{1}{\alpha_{\mathrm{N}}}}}\right) \frac{P_t G_{o,z}(P_t G_{o,z}\rho)^{\frac{2}{\alpha_{\mathrm{N}}}-1}}{\alpha_{\mathrm{N}}\sqrt{(P_t G_{o,z}\rho)^{\frac{2}{\alpha_{\mathrm{N}}}} - \zeta_k^2}}. \quad (18)$$

Similarly, the BSs can be mapped to a 1D PPP Ω_B^{1D} as given below

$$\Omega_B^{\mathrm{1D}} = \left\{\rho \triangleq \frac{r_{o,b}^\alpha}{P_t G_{o,b}}, b \in \Phi_B\right\}. \quad (19)$$

The CDF and PDF of the shortest distance ρ in Ω_B^{1D} are given in the following.

Lemma 4: The CDF of the shortest distance ρ in Ω_B^{1D} is expressed as

$$F_b(\rho) = 1 - \exp\Bigg[-\pi\lambda_B(\rho P_t G_{o,b})^{\frac{2}{\alpha_{\mathrm{N}}}} - \frac{2\pi\lambda_B}{\beta^2}\times \left[\left(1 - e^{-\beta(\rho P_t G_{o,b})^{\frac{1}{\alpha_{\mathrm{L}}}}}\left(1 + \beta(\rho P_t G_{o,b})^{\frac{1}{\alpha_{\mathrm{L}}}}\right)\right) - \left(1 - e^{-\beta(\rho P_t G_{o,b})^{\frac{1}{\alpha_{\mathrm{N}}}}}\left(1 + \beta(\rho P_t G_{o,b})^{\frac{1}{\alpha_{\mathrm{N}}}}\right)\right)\right]\Bigg]. \quad (20)$$

Proof: The proof is similar to that of [35, Lemma 1], which is omitted here. ∎

Corollary 2: The PDF of the shortest distance ρ in Ω_B^{1D} is described as

$$f_b(\rho) = \frac{d\Lambda[0,\rho]}{d\rho} \exp\Bigg[-\pi\lambda_B(\rho P_t G_{o,b})^{\frac{2}{\alpha_{\mathrm{N}}}} - \frac{2\pi\lambda_B}{\beta^2}\times \left[\left(1 - e^{-\beta(\rho P_t G_{o,b})^{\frac{1}{\alpha_{\mathrm{L}}}}}\left(1 + \beta(\rho P_t G_{o,b})^{\frac{1}{\alpha_{\mathrm{L}}}}\right)\right) - \left(1 - e^{-\beta(\rho P_t G_{o,b})^{\frac{1}{\alpha_{\mathrm{N}}}}}\left(1 + \beta(\rho P_t G_{o,b})^{\frac{1}{\alpha_{\mathrm{N}}}}\right)\right)\right]\Bigg], \quad (21)$$

where

$$\frac{d\Lambda[0,\rho]}{d\rho} = \frac{2\pi\lambda_B P_b G_{o,b}}{\alpha_{\mathrm{L}}}(\rho P_b G_{o,b})^{\frac{2}{\alpha_{\mathrm{L}}}-1} e^{-\beta(\rho P_t G_{o,b})^{\frac{1}{\alpha_{\mathrm{L}}}}} + \frac{2\pi\lambda_B P_b G_{o,b}}{\alpha_{\mathrm{N}}}(\rho P_b G_{o,b})^{\frac{2}{\alpha_{\mathrm{N}}}-1}\left(1 - e^{-\beta(\rho P_t G_{o,b})^{\frac{1}{\alpha_{\mathrm{N}}}}}\right). \quad (22)$$

Leveraging the above lemmas and corollaries, we derive the association probabilities of V2X and V2B links for the LPA scheme in the following theorem.

Theorem 2: In the LPA scheme, the association probabilities of V2X and V2B links are respectively expressed as

$$\mathcal{P}_{v2x}^{\mathrm{LPA}} = \int_0^\infty F_\rho(\rho) f_b(\rho) d\rho, \quad (23)$$

$$\mathcal{P}_{v2b}^{\mathrm{LPA}} = 1 - \mathcal{P}_{v2x}^{\mathrm{LPA}}, \quad (24)$$

where $F_\rho(\cdot)$ and $f_b(\cdot)$ are given in (15) and (21), respectively.

Proof: The proof of Theorem 2 is similar to that of Theorem 1. ∎

V. COP and SOP Analyses

In this section, we derive the COP for the SDA and LPA schemes where the typical vehicle can select either V2X nodes or BSs to receive messages. Meanwhile, the SOP is also analyzed in this section considering the eavesdroppers randomly distributed on the roads.

For either the SDA or LPA scheme, once a V2X node located at z is determined as the intended receiver, the received signal-to-interference-plus-noise ratio (SINR) at the receiver is given by

$$\gamma_{o,z} = \frac{P_t G_{o,z}|h_{o,z}|^2 r_{o,z}^{-\alpha}}{I_z + \sigma_0^2}, \quad (25)$$

where $I_z = I_z^{\mathrm{V}} + I_z^{\mathrm{B}}$ denotes the aggregate interference originating from the other V2X transmitters and BSs, with $I_z^{\mathrm{V}} = \sum_{u\in\Xi^T/o} P_t G_{u,z}|h_{u,z}|^2 r_{u,z}^{-\alpha}$ and $I_z^{\mathrm{B}} = \sum_{w\in\Phi_B^I} P_b G_{w,z}|h_{w,z}|^2 r_{w,z}^{-\alpha}$, Φ_B^I and P_b denote the PPP of the transmitting BSs and the transmit power, and σ_0^2 denotes the noise power.

Similarly, when a BS located at b is selected as the receiver, the received SINR is given by

$$\gamma_{o,b} = \frac{P_t G_{o,b}|h_{o,b}|^2 r_{o,b}^{-\alpha}}{I_b + \sigma_0^2}, \quad (26)$$

where $I_b = I_b^{\mathrm{V}} + I_b^{\mathrm{B}}$ is the aggregate interference originating from the other V2X transmitters and BSs, with $I_b^{\mathrm{V}} = \sum_{u\in\Xi^T/o} P_t G_{u,b}|h_{u,b}|^2 r_{u,b}^{-\alpha}$ and $I_b^{\mathrm{B}} = \sum_{w\in\Phi_B^I} P_b G_{w,b}|h_{w,b}|^2 r_{w,b}^{-\alpha}$.

For the potential eavesdroppers, the received SINR of the i-th eavesdropper is expressed as

$$\gamma_{o,e_i} = \frac{P_t G_{o,e_i}|h_{o,e_i}|^2 r_{o,e_i}^{-\alpha}}{I_e + \sigma_0^2}, \quad (27)$$

where $I_e = I_e^{\mathrm{V}} + I_e^{\mathrm{B}}$ is the aggregate interference originating from the other V2X transmitters and BSs, with $I_e^{\mathrm{V}} = \sum_{u\in\Xi^T/o} P_t G_{u,e_i}|h_{u,e_i}|^2 r_{u,e_i}^{-\alpha}$, and $I_e^{\mathrm{B}} = \sum_{w\in\Phi_B^I} P_b G_{w,e_i}|h_{w,e_i}|^2 r_{w,e_i}^{-\alpha}$.

A. COP for SDA Scheme

Conditioned on the intended receiver located at z belonging to V2X receivers, capacity of the main channel is expressed as $C_t = \log_2(1+\gamma_{o,z})$, where $\gamma_{o,z}$ is the SINR of the intended receiver given in (25). The connection outage event occurs when $R_t > C_t$, or equivalently, $\gamma_{o,z} < \beta_t$, where $\beta_t \triangleq 2^{R_t} - 1$ denotes the SINR threshold for connection outage. The COP

of the intended receiver is calculated as

$$\mathcal{P}_{co}^{v2x}\left(r_{o,z}\right)=\mathbb{P}\left[\gamma_{o,z}\leq\beta_t\right] \tag{28}$$
$$=\sum_{j\in\{\mathrm{L},\mathrm{N}\}}q_j\left(r_{o,z}\right)\mathbb{P}\left[\left|h_{o,z}\right|^2\leq\varpi_j\left(\sigma_0^2+I_z\right)\right]$$
$$\overset{(a)}{\geq}\sum_{j\in\{\mathrm{L},\mathrm{N}\}}q_j\left(r_{o,z}\right)\mathbb{E}_I\left[\left(1-e^{-A\varpi_j\left(\sigma_0^2+I_z\right)}\right)^m\right]$$
$$\overset{(b)}{=}\sum_{j\in\{\mathrm{L},\mathrm{N}\}}q_j\left(r_{o,z}\right)\sum_{l=0}^{m}(-1)^l\binom{m}{l}e^{-lA\varpi_j\sigma_0^2}\mathbb{E}_{I_z}\left[e^{-lA\varpi_j I_z}\right], \tag{29}$$

where $\varpi_j=r_{o,z}^{\alpha_j}\beta_t/(P_tG_{o,z})$, step (a) follows from the tight lower bound of a Gamma random variable as shown in [37], i.e., $\mathbb{P}\left[x<X\right]>\left(1-e^{-AX}\right)^m$, where $x\sim\Gamma\left(m,\frac{1}{m}\right)$ and $A=m\left(m!\right)^{-\frac{1}{m}}$, and step (b) is the result of the binomial expansion.

Similarly, for the intended receiver located at b belonging to BSs, the connection outage takes place when $\log_2\left(1+\gamma_{o,b}\right)<R_t$, i.e., $\gamma_{o,b}<\beta_t$, where $\gamma_{o,b}$ is given in (26). Hence, the COP of the intended receiver is derived as

$$\mathcal{P}_{co}^{v2b}\left(r_{o,b}\right)=\sum_{j\in\{\mathrm{L},\mathrm{N}\}}q_j\left(r_{o,b}\right)\sum_{l=0}^{m}(-1)^l\binom{m}{l}\times e^{-lA\varpi_j\sigma_0^2}\mathbb{E}_{I_b}\left[e^{-lA\varpi_j I_b}\right], \tag{30}$$

where $\varpi_j=r_{o,b}^{\alpha_j}\beta_t\Big/(P_tG_{o,b})$.

Note that the COPs in (28) and (30) contain the form of Laplace transform $\mathcal{L}_I(s)=\mathbb{E}_I\left[e^{-sI}\right]$. Hence, to calculate the COP, we only need to calculate the Laplace transform of the interference I_z and I_b, i.e., $\mathcal{L}_{I_z}(s)$ and $\mathcal{L}_{I_b}(s)$ at $s=lA\varpi_j$. Before that, we define an auxiliary function $\Upsilon\left(C,r\right)$ as given below, which can be used to express the Laplace transform conveniently.

$$\Upsilon\left(C,r\right)=1-\sum_{j\in\{\mathrm{L},\mathrm{N}\}}q_j\left(r\right)\left(1+Cm_j{}^{-1}r^{-\alpha_j}\right)^{-m_j}. \tag{31}$$

Note that $\Upsilon\left(C,r\right)$ can be regarded as: one minus the Laplace transform of the interference power when the distance between the receiver and interfere node is r, and the received interference power is $1/C$.

1) Laplace Transform of Interference from V2X Nodes: There are two kinds of lines (roads), namely, typical line L_0 and other lines $L_k\in\Phi_L$ in the V2X road system. Hence, We categorize the sources of interference into two disjoint sets: (i) the set of transmitting nodes located on L_0, and (ii) the set of transmitting nodes located on all the other lines $L_k\in\Phi_L$. We denote the interference from the two sets by $I_{\tau,0}^{\mathrm{V}}$ and $I_{\tau,k}^{\mathrm{V}}$ for $\tau\in\{z,b\}$, respectively. Based on this, the Laplace transform of interference can be given in the following lemma.

Lemma 5: For a V2B link, the Laplace transform of interference $I_{b,0}^{\mathrm{V}}$ can be given by

$$\mathcal{L}_{I_{b,0}^{\mathrm{V}}}(s)=\frac{1}{\pi}\int_0^{\pi}\exp\left[-2\mu^T\int_0^D\Upsilon\left(sP_tG_{u,b},r_{u,b}\right)dr_{o,u}\right]d\theta_0, \tag{32}$$

where $r_{u,b}=\sqrt{r_{o,u}^2+r_{o,b}^2-2r_{o,u}r_{o,b}\cos\theta_0}$.

Proof: The proof is given in Appendix B. ∎

Lemma 6: For a V2B link, the Laplace transform of interference $I_{b,k}^{\mathrm{V}}$ is expressed by

$$\mathcal{L}_{I_{b,k}^{\mathrm{V}}}(s)=\exp\Bigg(-2\pi\mu_L\int_0^D\Bigg[1-\exp\Bigg(-2\mu^T\times\int_0^{\sqrt{D^2-\zeta_k^2}}\Upsilon\left(sP_tG_{u,b},r\right)d\zeta_u\Bigg)\Bigg]\zeta_k d\zeta_k\Bigg), \tag{33}$$

where $r=\sqrt{\zeta_u^2+\zeta_k^2}$, and ζ_u is the distance between the interference at u and the intersection of line and its perpendicular line passing through the origin.

Proof: The proof is given in Appendix C. ∎

When the selected receiver is a V2X node, we can move the origin to this receiver since the PLP Φ_L is stationary and motion-invariant. Hence, we can derive the Laplace transform of interference from V2X nodes in the following lemma.

Lemma 7: For a V2X link, the Laplace transform of interference $I_{z,0}^{\mathrm{V}}$ can be given by

$$\mathcal{L}_{I_{z,0}^{\mathrm{V}}}(s)=\frac{1}{\pi}\int_0^{\pi}\exp\left(-2\mu^T\int_0^D\Upsilon\left(sP_tG_{u,z},r_{u,z}\right)dr_{o,u}\right)d\theta_0, \tag{34}$$

where $r_{u,z}=\sqrt{r_{o,u}^2+r_{o,z}^2-2r_{o,u}r_{o,z}\cos\theta_0}$.

Lemma 8: For a V2X link, the Laplace transform of interference $I_{z,k}^{\mathrm{V}}$ can be given by

$$\mathcal{L}_{I_{z,k}^{\mathrm{V}}}(s)=\exp\Bigg(-2\pi\mu_L\int_0^D\Bigg[1-\exp\Bigg(-2\mu^T\times\int_0^{\sqrt{D^2-\zeta_k^2}}\Upsilon\left(sP_tG_{u,z},r\right)d\zeta_u\Bigg)\Bigg]\zeta_k d\zeta_k\Bigg)\times\exp\left(-2\mu^T\int_0^D\Upsilon\left(sP_tG_{u,z},r_{u,z}\right)dr_{u,z}\right), \tag{35}$$

where $r=\sqrt{\zeta_u^2+\zeta_k^2}$.

Proof: The proofs of Lemmas 7 and 8 are similar to those of Lemmas 5 and 6. ∎

2) Laplace Transform of Interference from BSs: When the receiver is a BS, there exists a circular zone $\mathcal{S}_0\equiv\mathcal{B}\left(o,r_{o,b}\right)$ within which there are no BSs, where $r_{o,b}$ is the distance between the typical vehicle and the selected receiver. Obviously, it means that there is no interference originating from BSs in $\mathcal{S}_0$ for the receiver. For convenience, we translate the origin to the location of the receiver and define $\mathcal{S}_0$ with polar coordinates as

$$\mathcal{S}_0=\begin{cases}-\dfrac{\pi}{2}\leq\theta\leq\dfrac{\pi}{2}\\ r_{w,b}\leq 2r_{o,b}\cos\theta\end{cases}, \tag{36}$$

where w is the point in circular region $\mathcal{B}\left(o,r_{o,b}\right)$.

Based on the above analysis for $\mathcal{S}_0$, the Laplace transform of interference from BSs for the receiver (BS) is given in the following lemma.

Lemma 9: For the V2B link, the Laplace transform of

interference I_b^{B} is given by

$$\mathcal{L}_{I_b^{\mathrm{B}}}(s) = \exp\left(-\lambda_B \int_{\mathcal{B}(o,D)\setminus\mathcal{S}_0} \Upsilon\left(sP_tG_{w,b}, r_{w,b}\right) r_{w,b} dr_{w,b} d\theta_{w,b}\right). \tag{37}$$

Proof: Using the probability generating functional (PGFL) of a PPP and the same method of the proof for Lemma 6, Lemma 9 can be derived. ∎

If the receiver is a V2X node, there also exists a zone $\mathcal{S}_0 \equiv \mathcal{B}(o, r_{o,z})$ within which there are no BSs. With the same method in (36), we define $\mathcal{S}_0$ in polar coordinates as

$$\mathcal{S}_0 = \begin{cases} -\frac{\pi}{2} \le \theta \le \frac{\pi}{2} \\ r_{w,z} \le 2r_{o,z}\cos\theta \end{cases}, \tag{38}$$

where w denotes the point in circular region $\mathcal{B}(o, r_{o,z})$.

Similar to Lemma 9, the Laplace transform of interference from BSs for the receiver is shown in the following lemma.

Lemma 10: For the V2X link, the Laplace transform of interference I_z^{B} is given by

$$\mathcal{L}_{I_z^{\mathrm{B}}}(s) = \exp\left(-\lambda_B \int_{\mathcal{B}(o,D)\setminus\mathcal{S}_0} \Upsilon\left(sP_tG_{w,z}, r_{w,z}\right) r_{w,z} dr_{w,z} d\theta_{w,z}\right). \tag{39}$$

Proof: The proof is identical to the proof of Lemma 9. ∎

According to above analysis, the COP for the V2X and V2B links are given in the following.

Theorem 3: The COP of the V2X link for a given distance $r_{o,z}$ is derived as

$$\mathcal{P}_{co}^{v2x}(r_{o,z}) = \sum_{j\in\{\mathrm{L,N}\}} q_j(r_{o,z}) \sum_{l=0}^{m} \left[(-1)^l \binom{m}{l} e^{-lA\varpi_j\sigma_0^2} \times \mathcal{L}_{I_{z,0}^{\mathrm{V}}}(lA\varpi_j)\, \mathcal{L}_{I_{z,k}^{\mathrm{V}}}(lA\varpi_j)\, \mathcal{L}_{I_z^{\mathrm{B}}}(lA\varpi_j)\right], \tag{40}$$

where $\varpi_j = r_{0,z}^{\alpha_j}\beta_t/(P_tG_{o,z})$, $A = m_j(m_j!)^{-\frac{1}{m_j}}$, and $\mathcal{L}_{I_{v,0}^{\mathrm{V}}}(s)$, $\mathcal{L}_{I_{v,k}^{\mathrm{V}}}(s)$, and $\mathcal{L}_{I_v^{\mathrm{B}}}(s)$ are given in (34), (35), and (39), respectively.

Theorem 4: The COP of the V2B link for a given distance $r_{o,b}$ is derived as

$$\mathcal{P}_{co}^{v2b}(r_{o,b}) = \sum_{j\in\{\mathrm{L,N}\}} q_j(r_{o,b}) \sum_{l=0}^{m} \left[(-1)^l \binom{m}{l} e^{-lA\varpi_j\sigma_0^2} \times \mathcal{L}_{I_{b,0}^{\mathrm{V}}}(lA\varpi_j)\mathcal{L}_{I_{b,k}^{\mathrm{V}}}(lA\varpi_j)\, \mathcal{L}_{I_b^{\mathrm{B}}}(lA\varpi_j)\right], \tag{41}$$

where $\varpi_j = r_{0,b}^{\alpha_j}\beta_t\big/(P_tG_{o,b})$, and $\mathcal{L}_{I_{b,0}^{\mathrm{V}}}(s)$, $\mathcal{L}_{I_{b,k}^{\mathrm{V}}}(s)$, and $\mathcal{L}_{I_b^{\mathrm{B}}}(s)$ are given in (32), (33), and (37), respectively.

We should point out that although (40) and (41) are expressed in the form of Laplace transform, they are easy to compute since the integral intervals are finite. Besides, owing to the great benefits brought by the stochastic geometry theory, increasing the densities of V2X nodes and BSs will not consume a higher computational cost. By using the total probability law, the overall COP of the secure uplink transmission under the SDA scheme can be easily calculated as follows,

$$\mathcal{P}_{co}^{\mathrm{SDA}} = P_{v2x}^{\mathrm{SDA}} \int_0^\infty \mathcal{P}_{co}^{v2x}(r_{o,z})\, f_z(r_{0,z})\, dr_{o,z} + P_{v2b}^{\mathrm{SDA}} \int_0^\infty \mathcal{P}_{co}^{v2b}(r_{o,b})\, f_b(r_{0,b})\, dr_{o,b}, \tag{42}$$

where $P_{\mathrm{V2X}}^{\mathrm{SDA}}$, $P_{\mathrm{V2B}}^{\mathrm{SDA}}$, $\mathcal{P}_{co}^{v2x}(\cdot)$, $\mathcal{P}_{co}^{v2b}(\cdot)$, $f_z(\cdot)$, and $f_b(\cdot)$ are given in (8), (9), (40), (41), (5), and (7), respectively.

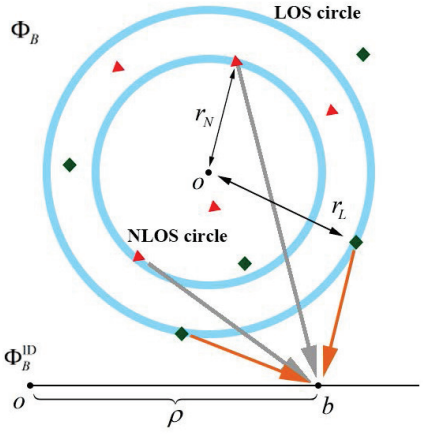

Fig. 3. Illustration of the mapping relationship between the BSs in 2D plane and the node in 1D PPP Ω_b^{1D}, where red triangles and green squares respectively denote the BSs with NLOS and LOS links, and arrows denote mapping relationship.

B. COP for LPA scheme

To facilitate the analysis of the distribution of the optimal receiver for the LPA scheme, we resort to the Mapping theory to map the randomly distributed wireless nodes in the 2D plane, including V2X nodes and BSs, into new 1D PPPs. Considering a given node in the mapped 1D PPP with distance ρ from the original, for deriving the COP, we need to determine the distance between the node and the origin on the original 2D plane, as well as the link status of the communication, which will subsequently be used to derive the Laplace transform of interference. Revisiting (14) and (19), we can obtain the following lemma.

Lemma 11: Conditioned on a given distance ρ between the origin and a node in the mapped PPP Ω_k^{1D} or Ω_b^{1D}, the corresponding distance in the original PPP Ξ^R or Φ_B with LOS and NLOS links can be respectively given by

$$r_{\mathrm{L}} = (P_tG_{o,\tau}\rho)^{\frac{1}{\alpha_{\mathrm{L}}}},\ r_{\mathrm{N}} = (P_tG_{o,\tau}\rho)^{\frac{1}{\alpha_{\mathrm{N}}}},\ \tau \in \{z, b\}. \tag{43}$$

Proof: The proof of Lemma 11 can be directly obtained from (14) and (19). ∎

In order to derive the COP, we need to calculate the probability that the link is LOS or NLOS between the point in the origin point process which is corresponding to a point in the mapped PPP and the origin.

Lemma 12: Conditioned on a certain distance ρ between the origin and a node in the mapped PPP Ω_k^{1D} or Ω_b^{1D}, the

probabilities of the corresponding node in the original PPP Ξ^R or Φ_B being a LOS and NLOS links can be respectively expressed as

$$\mathcal{P}_{\mathrm{L}}(\rho)=\frac{r_{\mathrm{L}}e^{-\beta r_{\mathrm{L}}}}{r_{\mathrm{L}}e^{-\beta r_{\mathrm{L}}}+r_{\mathrm{N}}\left(1-e^{-\beta r_{\mathrm{N}}}\right)},\ \mathcal{P}_{\mathrm{N}}(\rho)=1-\mathcal{P}_{\mathrm{L}}(\rho), \tag{44}$$

where r_{L} and r_{N} are given in (43).

Proof: As shown in Fig. 3, for the mapped PPP Ω_b^{1D}, we can find that BSs whose communication links are LOS or NLOS can all be mapped to a same node b in Ω_B^{1D}. Condition on a given distance ρ in Ω_B^{1D}, the location of BSs mapped to b with LOS link in 2D plane is distributed on a circle with radius r_{L}, and the location of BSs mapped to b with NLOS link is distributed on a circle with radius r_{N}. For convenience, we define the circles with radius r_{L} and r_{N} respectively as LOS circle and NLOS circle. Hence, the probability of the node b remapped to the nodes in LOS circle can be denoted as the ratio of the number of nodes on the LOS circle mapped to b to the total number of nodes mapped to b, which is given by

$$\mathcal{P}_{\mathrm{L}}(\rho)\triangleq\frac{\bar{N}_{\mathrm{L}}}{\bar{N}_{\mathrm{L}}+\bar{N}_{\mathrm{N}}}, \tag{45}$$

where $\bar{N}_{\mathrm{L}}$ and $\bar{N}_{\mathrm{N}}$ denote the number of nodes on the LOS and NLOS circles mapped to b, respectively.

We assume that the width of the LOS and NLOS circles is dr ($dr\to 0$), i.e., we treat each circle as an annulus, and the difference between its outside diameter and inside diameter is dr. We can easily calculate that the areas of LOS and NLOS annuluses are $2\pi r_{\mathrm{L}}dr$ and $2\pi r_{\mathrm{N}}dr$, respectively. Leveraging the property of a PPP, the average numbers of nodes on LOS circle and NLOS circle mapped to b are calculated as

$$\bar{N}_{\mathrm{L}}=2\pi r_{\mathrm{L}}e^{-\beta r_{\mathrm{L}}}\mu^R dr,\ \bar{N}_{\mathrm{N}}=2\pi r_{\mathrm{N}}(1-e^{-\beta r_{\mathrm{N}}})\mu^R dr, \tag{46}$$

where $e^{-\beta r_{\mathrm{L}}}\mu^R$ and $(1-e^{-\beta r_{\mathrm{N}}})\mu^R$ denotes the densities of the BSs with LOS link on LOS circle and with NLOS link on NLOS circle, respectively.

Inserting (46) into (45), we will get (44).

Similarly, we can treat the mapping relationship between the V2X node on the roads and the node in Ω_k^{1D} with the same method. The difference is that the possible mapping nodes on a 2D plane need to be at the intersection of circles and the road. After derivation, we will obtain the same result as the mapping process of BSs in (44). ∎

Conditioned on the distance ρ, the COP of V2X and V2B link can be uniformly expressed as

$$\mathcal{P}_{co}^{\mathrm{V2X/V2B}}(\rho)=\sum_{j\in\{\mathrm{L},\mathrm{N}\}}\mathcal{P}_j(\rho)\sum_{l=0}^{m}\binom{m}{l}(-1)^l e^{-lA\rho\beta_t\sigma_0^2}\times \mathbb{E}_{I_\tau}\left[e^{-lA\rho\beta_t I_\tau}\right],\ \tau\in\{z,b\}. \tag{47}$$

Similar to the analysis for the SDA scheme, we will next discuss the Laplace transform of the interference for the LPA scheme.

1) Lapalce Transform of Interference from V2X nodes: Since the locations of the V2X transmitters and V2X receivers are modeled as two independent Cox processes, the Laplace transform of the interference from V2X nodes for the LPA scheme does not rely on the specific association scheme, such that is identical to that for the SDA scheme.

2) Laplace Transform of Interference from BSs: When the receiver is a V2X node, for arbitrary interference BS located at w, we can confirm that

$$P_tG_{o,w}r_{o,w}^{-\alpha_g}<\underbrace{P_tG_{o,z}r_{o,z}^{-\alpha}}_{1/\rho}\Leftrightarrow\rho P_tG_{o,w}<r_{o,w}^{\alpha_g}$$
$$\Leftrightarrow r_{o,w}>\left(\rho P_tG_{o,w}\right)^{\frac{1}{\alpha_g}},\quad g\in\{\mathrm{L},\mathrm{N}\}, \tag{48}$$

where $g\in\{\mathrm{L},\mathrm{N}\}$ denotes the link status between the selected receiver and an interference BS.

Obviously, the minimum distance $r_{o,w}$ is different for LOS and NLOS links. We decouple the aggregate interference of BSs into LOS and NLOS components, and derive their Laplace transform independently. The density of the interference BSs is given as

$$\hat{\lambda}_B^g=q_g(r_{w,z})\lambda_B\mathbb{I}\left[r_{o,w}>\left(\rho P_tG_{o,w}\right)^{\frac{1}{\alpha_g}}\right], \tag{49}$$

where $r_{w,z}=\sqrt{r_{o,w}^2+r_{o,z}^2-2r_{o,w}r_{o,z}\cos\theta_{o,w}}$ and $\theta_{o,w}$ is an angle formed by the target receiver, typical vehicle, and the interference node. It is worth noting that, $r_{o,z}$ denotes the distance between the typical vehicle and target receiver as expressed in (43), which is different for the main channel with LOS and NLOS links.

The following lemmas give the Laplace transform of interference from BSs.

Lemma 13: For the V2X link, the Laplace transform of interference $\mathcal{L}_{I_z^{\mathrm{B}}}^j$ can be described as

$$\mathcal{L}_{I_z^{\mathrm{B}}}^j(x)=\mathcal{L}_{I_z^{\mathrm{B}},\mathrm{L}}^j(x)\,\mathcal{L}_{I_z^{\mathrm{B}},\mathrm{N}}^j(x), \tag{50}$$

where

$$\mathcal{L}_{I_z^{\mathrm{B}},g}^j=\exp\left(-\int_{\mathcal{B}(o,D)}\left[1-\left(1+\frac{s}{m}P_bG_{w,z}r_{w,z}^{-\alpha_g}\right)^{-m}\right]\times\hat{\lambda}_B^g r_{o,w}dr_{o,w}d\theta_{o,w}\right),\ g\in\{\mathrm{L},\mathrm{N}\}, \tag{51}$$

$\hat{\lambda}_B^g$ is given in (49), and $j\in\{\mathrm{L},\mathrm{N}\}$ denotes the main channel link status.

Proof: The proof is similar to that for Lemma 10. ∎

When the receiver is a BS, the density of the interference BSs can be expressed by

$$\hat{\lambda}_B^g=q_g(r_{w,b})\lambda_B\mathbb{I}\left[r_{o,w}>\left(\rho P_tG_{o,w}\right)^{\frac{1}{\alpha_g}}\right], \tag{52}$$

with $r_{w,b}=\sqrt{r_{o,b}^2+r_{o,w}^2-2r_{o,b}r_{o,w}\cos\theta_{o,w}}$, where $r_{o,b}$ is also defined in (43).

Lemma 14: For the V2B link, the Laplace transform of interference $\mathcal{L}_{I_b^{\mathrm{B}}}^j$ can be described as

$$\mathcal{L}_{I_b^{\mathrm{B}}}^j(x)=\mathcal{L}_{I_b^{\mathrm{B}},\mathrm{L}}^j(x)\,\mathcal{L}_{I_b^{\mathrm{B}},\mathrm{N}}^j(x), \tag{53}$$

where

$$\mathcal{L}^{j}_{I^{\mathrm{B}}_{b},g}(s)=\exp\Bigg(-\int_{\mathcal{B}(o,D)}\left[1-\left(1+\frac{s}{m}P_bG_{w,b}r_{w,b}^{-\alpha_g}\right)^{-m}\right]\times\hat{\lambda}^{g}_{B}r_{o,w}dr_{o,w}d\theta_{o,w}\Bigg),\ g\in\{\mathrm{L},\mathrm{N}\},\tag{54}$$

Based on the above analyses, the following theorems give the COPs of V2X and V2B links.

Theorem 5: The COP of the V2X link for a given distance ρ between the origin and the node in the mapped PPP Φ^{1D}_{k} is derived as

$$\mathcal{P}^{v2x}_{co}(\rho)=\sum_{j\in\{\mathrm{L},\mathrm{N}\}}\mathcal{P}_j(\rho)\sum_{l=0}^{m}\binom{m}{l}(-1)^{l}e^{-lA\rho\beta_t\sigma_0^2}\times\mathcal{L}_{I^{\mathrm{V}}_{z,0}}(lA\rho\beta_t)\,\mathcal{L}_{I^{\mathrm{V}}_{z,k}}(lA\rho\beta_t)\,\mathcal{L}^{j}_{I^{\mathrm{B}}_{z}}(lA\rho\beta_t),\tag{55}$$

where $\mathcal{L}_{I^{\mathrm{V}}_{z,0}}(\cdot)$, $\mathcal{L}_{I^{\mathrm{V}}_{z,k}}(\cdot)$, and $\mathcal{L}^{j}_{I^{\mathrm{B}}_{z}}(\cdot)$ are respectively given in (34), (35), and (50).

Theorem 6: The COP of the V2B link for a given distance ρ between the origin and the node in mapped point process is derived as

$$\mathcal{P}^{v2b}_{co}(\rho)=\sum_{j\in\{\mathrm{L},\mathrm{N}\}}\mathcal{P}_j(\rho)\sum_{l=0}^{m}\binom{m}{l}(-1)^{l}e^{-lA\rho\beta_t\sigma_0^2}\times\mathcal{L}_{I^{\mathrm{V}}_{b,0}}(lA\rho\beta_t)\,\mathcal{L}_{I^{\mathrm{V}}_{b,k}}(lA\rho\beta_t)\,\mathcal{L}^{j}_{I^{\mathrm{B}}_{b}}(lA\rho\beta_t),\tag{56}$$

where $\mathcal{L}_{I^{\mathrm{V}}_{b,0}}(\cdot)$, $\mathcal{L}_{I^{\mathrm{V}}_{b,k}}(\cdot)$, and $\mathcal{L}^{j}_{I^{\mathrm{B}}_{z}}(\cdot)$ are respectively given in (32), (33), and (53).

Theorem 7: The overall COP for the LPA scheme can be expressed by

$$\mathcal{P}^{\mathrm{LPA}}_{co}=P^{\mathrm{LPA}}_{v2x}\int_0^{\infty}\mathcal{P}^{v2x}_{co}(\rho)\,f_{\rho}(\rho)\,d\rho+P^{\mathrm{LPA}}_{v2b}\int_0^{\infty}\mathcal{P}^{v2b}_{co}(\rho)\,f_b(\rho)\,d\rho,\tag{57}$$

where P^{LPA}_{v2x}, P^{LPA}_{v2b}, $\mathcal{P}^{v2x}_{co}(\cdot)$, $\mathcal{P}^{v2b}_{co}(\cdot)$, $f_{\rho}(\cdot)$, and $f_b(\cdot)$ are given in (23), (24), (55), (56), (17), and (21), respectively.

C. SOP

The secrecy outage event takes place if only the capacity of the most detrimental wiretap channel exceeds the rate redundancy R_e, i.e., $\log_2(1+\max_{e_i\in\Phi_e}\gamma_{o,e_i})>R_e$, or equivalently, $\max_{e_i\in\Phi_e}\gamma_{o,e_i}>\beta_e$, where $\beta_e\triangleq 2^{R_e}-1$ denotes the SINR threshold for secrecy outage. Note that the SOP is solely determined by the channels and distances between the typical vehicle and eavesdroppers, which is irrelevant to the adopted association scheme, we will direct derive the SOP with no need for considering the association schemes. We express the SOP for both SDA and LPA schemes uniformly in the following theorem.

Theorem 8: The SOP for both the SDA and LPA schemes can be given by

$$\mathcal{P}_{so}=1-\exp\Bigg(-2\pi\mu_L\int_0^{D}\Bigg(1-\exp\Bigg(-2\mu^{E}\int_0^{\sqrt{D^2-\zeta_k^2}}(1-p_{e_i})\,dr_{e_i}\Bigg)\Bigg)d\zeta_k\Bigg),\tag{58}$$

where

$$p_{e_i}=\sum_{j\in\{\mathrm{L},\mathrm{N}\}}q_j(r_{o,e_i})\sum_{l=0}^{m}(-1)^{l}\binom{m}{l}e^{-lA\varpi_j\sigma_0^2}\times\mathcal{L}_{I^{\mathrm{V}}_{e_i,k}}(s)\,\mathcal{L}_{I^{\mathrm{V}}_{e_i,0}}(s)\,\mathcal{L}_{I^{\mathrm{B}}_{e_i}}(s),\tag{59}$$

$$\mathcal{L}_{I^{\mathrm{V}}_{e_i,k}}(s)=\exp\Bigg(-2\pi\mu_L\int_0^{D}\Bigg[1-\exp\Bigg(-2\mu^{T}\times\int_0^{\sqrt{D^2-\zeta_k^2}}\Upsilon(sP_tG_{u,e_i},r_1)\,d\zeta_u\Bigg)\Bigg]\zeta_k d\zeta_k\Bigg)\times\exp\Bigg(-2\mu^{T}\int_0^{D}\Upsilon(sP_tG_{u,e_i},r_{u,e_i})\,dr_{u,e_i}\Bigg),\tag{60}$$

$$\mathcal{L}_{I^{\mathrm{V}}_{e_i,0}}(s)=\frac{1}{\pi}\int_0^{\pi}\exp\left[-2\mu^{T}\int_0^{D}\Upsilon(sP_tG_{u,e_i},r_2)\,dr_{o,u}\right]d\theta_0,\tag{61}$$

$$\mathcal{L}_{I^{\mathrm{B}}_{e_i}}(s)=\exp\left(-\lambda_B\int_0^{2\pi}\int_0^{D}\Upsilon(sP_tG_{w,e_i},r_{w,e_i})\,r_{w,e_i}dr_{w,e_i}d\theta\right),\tag{62}$$

$r_1=\sqrt{\zeta_u^2+\zeta_k^2}$, $r_2=\sqrt{r_{o,e_i}^2+r_{o,u}^2-2r_{o,e_i}r_{o,u}\cos\theta_0}$, and $r_{o,e_i}=\sqrt{r_{e_i}^2+\zeta_k^2}$.

Proof: The proof is given in Appendix D. ■

Although the SOP $\mathcal{P}_{so}$ given in (58) is complicated to analyze, one can easily confirm that it will decrease with the SINR threshold β_e, the density of V2X transmitters μ^T, and the density of BSs λ_B, and increase with the density of eavesdroppers μ^E. In what follows, we further perform asymptotic analyses on $\mathcal{P}_{so}$ by examining different cases of the road density λ_L, or equivalently the point density μ_L, as well as the eavesdropper density μ^E.

1) For the case $\mu_L\to 0$ or $\mu^E\to 0$, we have $\mathcal{P}_{so}\to 0$. This is intuitive since a secrecy outage event will not occur when there are no roads or eavesdroppers.
2) For the case $\mu_L\to\infty$ and $\mu_E>0$, we have $\mathcal{P}_{so}\to 1$. This can be understood once one realizes that as the road density goes to infinity, the most harmful eavesdropper could be arbitrarily close to the typical vehicle, resulting in secrecy leakage with probability one.
3) For the case $\mu_L>0$ and $\mu_E\to\infty$, we have $\mathcal{P}_{so}\to 1-e^{-2\pi\mu_L D}$, which appears to be a concise function of the density μ_L. Different from the second case, even if the density μ_E of eavesdroppers on each road goes to infinity, the SOP will tend to be a constant less than one. This is because, the roads where the eavesdroppers reside might not pass through the origin such that no eavesdropper can be arbitrarily close to the typical vehicle.
4) For the case $\mu_L\to\infty$ and $\mu^E\to 0$ with $\mu_L\mu^E=\bar{\mu}$, we can obtain a closed-form upper bound for the SOP in the following corollary.

Corollary 3: Considering $\mu_L \to \infty$ and $\mu^E \to 0$ with $\mu_L \mu^E = \bar{\mu}$, the SOP $\mathcal{P}_{so}$ is asymptotically upper bounded by $1 - e^{-\pi^2 D^2 \bar{\mu}}$.

Proof: Note that $\lim_{\mu_L \to \infty} p_{ei} \to 0$, substituting which into (58) yields

$$\begin{aligned}
&\mathcal{P}_{so}^{\mu_L \to \infty, \mu^E \to 0} \\
&= 1 - \exp\left(-2\pi\mu_L \int_0^D \left(1 - e^{-2\mu^E \sqrt{D^2 - \zeta^2}}\right) d\zeta \right) \\
&\overset{(a)}{\leq} 1 - \exp\left(-4\pi\mu_L \mu^E \int_0^D \sqrt{D^2 - \zeta^2} d\zeta \right) \\
&\overset{(b)}{=} 1 - e^{-\pi^2 D^2 \bar{\mu}}, \qquad (63)
\end{aligned}$$

where step (a) follows from the inequality $1 - e^{-x} < x$ and step (b) holds by using a substitution $\zeta = D\sin(t)$. ∎

We show that the obtained asymptotic upper bound for SOP exponentially increases with the equivalent density $\bar{\mu}$ of the eavesdroppers on the 2D plane.

VI. Numerical Result and Discussion

In this section, we provide theoretical and Monte-Carlo simulation results to validate the analysis and proposed theorems and lemmas. We analyze the secrecy metrics as functions of networks parameters, and provide various insights. Unless otherwise specified, we set the parameters as $P_t = P_b = 0$ dBw, $\sigma_0^2 = 0$ dBm, $M_b = 15$ dB, $m_b = -15$ dB, $\theta_b = \pi/20$, $M_z = 10$ dB, $m_z = -10$ dB, $\theta_z = \pi/6$, $\beta = 0.15$, $\alpha_{\mathrm{L}} = 2.1$, $\alpha_{\mathrm{N}} = 3.5$, $\mu^R = 1$, $\mu^E = 1$, and $m = 4$. Note that the unit for the densities of BSs and V2X nodes is $node/10m^2$.[5]

A. Association Probabilities Analysis

Fig. 4 plots the association probabilities of V2X nodes for SDA and LPA schemes $\mathcal{P}_{v2x}^{\mathrm{SDA}}\left(\mathcal{P}_{v2x}^{\mathrm{LPA}}\right)$ versus the density of V2X receivers μ^R. We observe that, with the increase of μ^R, the typical vehicle prefers to access the V2X nodes rather than to the BSs in both association schemes. Besides, a larger μ_L leads to a larger $\mathcal{P}_{v2x}^{\mathrm{SDA}}\left(\mathcal{P}_{v2x}^{\mathrm{LPA}}\right)$, and a larger λ_B leads a smaller $\mathcal{P}_{v2x}^{\mathrm{SDA}}\left(\mathcal{P}_{v2x}^{\mathrm{LPA}}\right)$.

B. COP and SOP Analysis

Fig. 5 and Fig. 6 plot the overall COP of the SDA scheme $\mathcal{P}_{co}^{\mathrm{SDA}}$ and the LPA scheme $\mathcal{P}_{co}^{\mathrm{LPA}}$ versus the SINR threshold β_t, respectively. The Monte-Carlo simulation results can well math the theoretical values. We see that the curves in the two figures are quite similar. Take Fig. 5 as an example, and some observation can be made: 1) The overall COP $\mathcal{P}_{co}^{\mathrm{SDA}}$ increases with the increase of β_t. 2) When the densities of roads μ_L and BS λ_B are fixed, a larger density of V2X transmitter leads to a larger overall COP. 3) When the densities of V2X transmitters μ^T and roads μ_L are determined, increasing λ_B will incur a larger overall COP. 4) When the densities of BSs and V2X transmitters are fixed, the overall COP with large road density is smaller than that of lower one in low SINR threshold range. Besides, the LPA scheme has a smaller COP with the same system parameters, compared with the SDA scheme, since the interference power for both schemes is the same and the receiver in the LPA scheme can always obtain the maximum received power. Fig. 7 depicts the SOP $\mathcal{P}_{so}$ versus the SINR threshold β_e. It can be observed that: 1) $\mathcal{P}_{so}$ decrease with β_e; 2) A larger BS density λ_B or a larger density of V2X transmitters μ^T leads to a smaller SOP because of the increase of interference for the eavesdroppers; 3) The increase μ_L increases the SOP, which indicates that a more intensive road construction is harmful to secrecy performance, although the densities of both μ^T and μ^E are increased.

[5]For tractability, we ignore the exact size of vehicles. However, choosing a proper vehicle density can simulate well a practical V2X network with general vehicle sizes, e.g., a small vehicle density can reflect a sparse network or large-size vehicles, vice versa. In fact, when the size of vehicles cannot be omitted, e.g., to avoid vehicle collision in a dense network, we can use the Matérn hard-core process (HCPP) to model the locations of vehicles as done in [29], where the Matérn HCPP can be formed as a repulsive PPP with any two nodes separated by a radius characterizing the vehicle size.

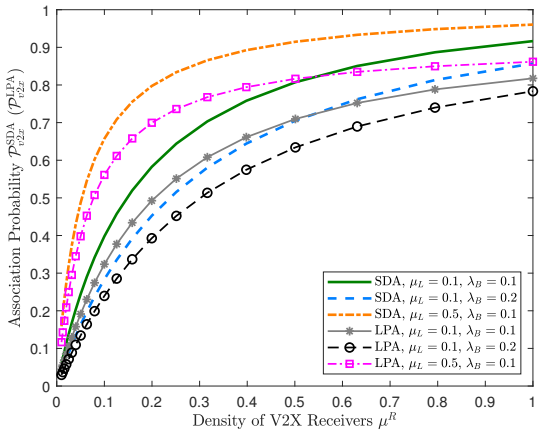

Fig. 4. Association probability $\mathcal{P}_{v2x}^{\mathrm{SDA}}(\mathcal{P}_{v2x}^{\mathrm{LPA}})$ v.s. the density of V2X receivers μ^R, with $G_{o,z} = G_{o,b} = 1$.

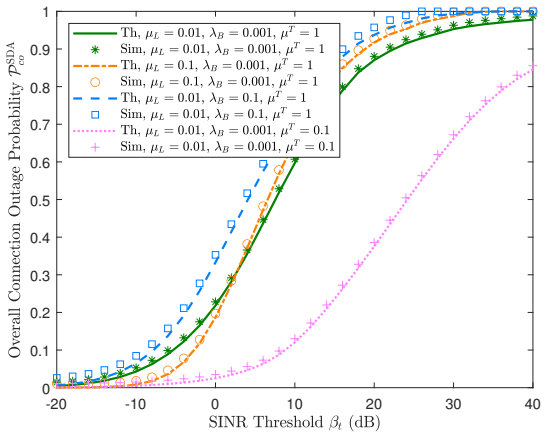

Fig. 5. The overall COP $\mathcal{P}_{co}^{\mathrm{SDA}}$ v.s. SINR threshold β_t.

C. Secrecy Throughput Analysis

Fig. 8 depicts the secrecy throughput Ψ of SDA and LPA schemes as a function of secrecy rate R_s. We see that Φ for each association scheme first increases and then decreases

This article has been accepted for publication in IEEE Transactions on Wireless Communications. This is the author's version which has not been fully edited and content may change prior to final publication. Citation information: DOI 10.1109/TWC.2022.3179706

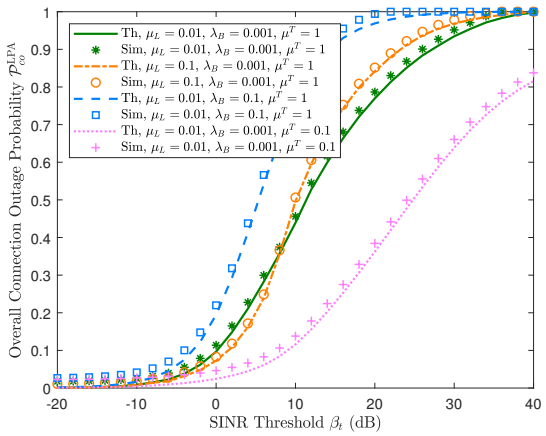

Fig. 6. Overall COP $\mathcal{P}_{co}^{\mathrm{LPA}}$ v.s. SINR threshold β_t.

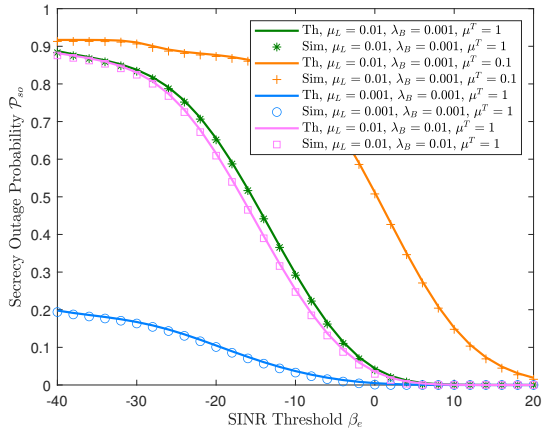

Fig. 7. SOP $\mathcal{P}_{so}$ v.s. SINR threshold β_e.

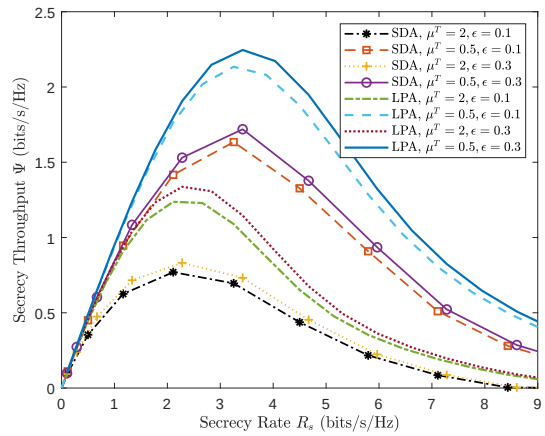

Fig. 8. Secrecy throughput Ψ v.s. secrecy rate R_s, with $\mu_L = 0.01$ and $\lambda_B = 0.1$.

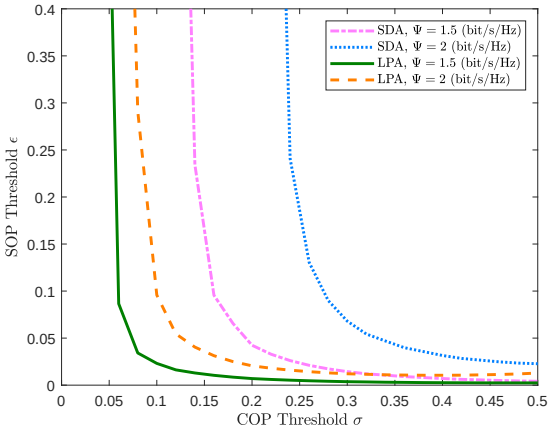

Fig. 9. SOP threshold ϵ and COP threshold σ vs. secrecy throughput Ψ, with $\mu_L = 0.01$ and $\lambda_B = 0.1$.

as R_s increases, and there exists a unique optimal R_s that achieve the maximal Ψ. The underlying reason is that, in order to improve secrecy throughput, we generally prefer to set a large R_s, whereas an overly large R_s will incur a large COP, thus harming secrecy throughput. Meanwhile, according to this figure, we can find that: 1) For both SDA and LPA schemes, the increase of SOP threshold ϵ increases the secrecy throughput. 2) With the same system parameters, we observe that the LPA scheme is superior to the SDA scheme in terms of secrecy throughput. 3) A larger density of V2X transmitter, i.e., interference node, will lead to a smaller secrecy throughput.

Fig. 9 illustrates the relationship between secrecy throughput Ψ and SOP threshold ϵ and COP threshold σ. The following insights can be provided: 1) A non-trivial trade-off between reliability and secrecy is disclosed for both SDA and LPA schemes, and we can see that as σ increases along the curve with a constant secrecy throughput, the value of ϵ becomes smaller, i.e., a more stringent secrecy constraint can be satisfied. 2) For both SDA and LPA schemes, the curve moves to the right as Ψ increases, which indicates a shrunken feasible region for σ and ϵ. This is as expected, since a higher secrecy throughput is achieved at the cost of sacrificing either reliability or secrecy performance. 3) For the curves with the same secrecy throughput, the LPA scheme can satisfy a tighter reliability or secrecy constraint (i.e., a lower COP threshold or a lower SOP threshold) than the SDA scheme, which demonstrates the superiority of the LPA scheme in safeguarding the physical-layer security for the mmWave C-V2X networks under investigation.

VII. Conclusions

In this paper, we have investigated the physical-layer security of uplink transmissions in the mmWave C-V2X networks. A comprehensive and tractable analytical framework for both reliability and secrecy performance of the secure transmission has been presented. Specifically, we have proposed two association schemes, namely, the SDA and LPA schemes, to connect an arbitrary vehicle to either V2X nodes or BSs. New analytical expressions of the association probabilities, COP, and SOP have been derived for both association schemes. Simulation results have revealed the impacts of system parameters on the COP, SOP, and secrecy throughput for both the SDA and LPA schemes, and demonstrated the advantage of the LPA scheme in terms of secrecy throughput enhancement compared with the SDA scheme.

APPENDIX A
PROOF OF LEMMA 3

Recalling the definition of the mapped PPP Ω_k with parameters (ζ_k, θ) and μ^R, the intensity of Ω_k can be calculated as

$$\Lambda_{\zeta_k}[0,\rho] = \int_0^{\sqrt{(P_t G_{o,z}\rho)^{\frac{2}{\alpha_{\mathrm{L}}}} - \zeta_k^2}} 2\mu^R e^{-\beta\sqrt{\zeta_k^2+\zeta_z^2}} d\zeta_z + \int_0^{\sqrt{(P_t G_{o,z}\rho)^{\frac{2}{\alpha_{\mathrm{N}}}} - \zeta_k^2}} 2\mu^R \left(1 - e^{-\beta\sqrt{\zeta_k^2+\zeta_z^2}}\right) d\zeta_z, \quad (64)$$

Using the void probability of PPP [39] and along with (64), we have the CDF of the nearest distance ρ in the mapped PPP Ω_k, i.e.,

$$F_{\rho,L_k}(\rho) \triangleq 1 - \mathbb{P}\left[\rho < r^*_{L_k}\right] = 1 - e^{-\Lambda_{\zeta_k}[0,\rho]}, \quad (65)$$

where $r^*_{L_k}$ denotes the distance between the origin and the nearest node in the mapped PPP Ω_k.

When $\zeta_k = 0$, we will obtain the CDF of the nearest distance ρ in Ω_0, which is mapped from the 1D PPP on the typical line L_0.

Considering the receivers on each line, the CDF of the nearest distance ρ can be expressed as

$$\begin{aligned} F_\rho(\rho) &= \mathbb{P}\left[\rho \geq \min_k \left\{ r^*_{L_k} \middle| L_k \in \Phi_{L_0} \right\}\right] \\ &= 1 - \mathbb{P}\left[\rho < \min_k \left\{ r^*_{L_k} \middle| L_k \in \Phi_{L_0} \right\}\right] \\ &\overset{(a)}{=} 1 - \mathbb{P}\left[\rho < r^*_{L_0}\right] \mathbb{E}_{\Phi_L}\left[\prod_{L_k \in \Phi_L} \mathbb{P}\left[\rho < r^*_{L_k}\right]\right], \end{aligned} \quad (66)$$

where step (a) separates the typical line from the PLP Φ_{L_0}, and $\mathbb{P}\left[\rho < r^*_{L_k}\right]$ and $\mathbb{P}\left[\rho < r^*_{L_0}\right]$ can be obtained from (65).

Before deriving the expression of $F_\rho(\rho)$, we need to calculate $\mathbb{E}_{\Phi_L}\left[\prod_{L_k \in \Phi_L} \mathbb{P}\left[\rho < r^*_{L_k}\right]\right]$ in (66),

$$\begin{aligned} &\mathbb{E}_{\Phi_L}\left[\prod_{L_k \in \Phi_L} \mathbb{P}\left[\rho < r^*_{L_k}\right]\right] \\ &\overset{(b)}{=} \sum_{n=0}^{\infty} \mathbb{P}\left[N(\Phi_L) = n\right] \left(\mathbb{E}_{\zeta_k}\left[\mathbb{P}\left[\rho < r^*_{L_k}\right]\right]\right)^n \\ &\overset{(c)}{=} \sum_{n=0}^{\infty} \frac{e^{-2\pi\mu_L D}(2\pi\mu_L D)^n}{n!} \left[\frac{1}{D}\int_0^D \left(1 - F_{\rho,L_k}(\rho)\right) d\zeta_k\right]^n \\ &= e^{-2\pi\mu_L D} \sum_{n=0}^{\infty} \frac{1}{n!} \left[2\pi\mu_L \int_0^D \left(1 - F_{\rho,L_k}(\rho)\right) d\zeta_k\right]^n \\ &= \exp\left(-2\pi\mu_L \int_0^D F_{\rho,L_k}(\rho)\, d\zeta_k\right), \end{aligned} \quad (67)$$

where $N(\cdot)$ denotes the element number of a Poisson process, step (b) follows from the independence of randomly distributed lines, and step (c) uses the probability for Poisson distribution.

Inserting (65) and (67) into (66), the CDF can be obtained as (15).

APPENDIX B
PROOF OF LEMMA 5

Since the typical line L_0 is determined randomly, all the spatial location relationships between the typical line and receiver should be considered. We define θ_0 as the angle between the typical line and horizontal line, and it is obvious that θ_0 follows the uniform distribution $U(0,\pi)$. Conditioned on θ_0, the Laplace transform of interference from the typical line is given by

$$\begin{aligned} &\mathcal{L}_{I^{\mathrm{V}}_{b,0}|\theta_0}(s) \\ &= \mathbb{E}_{\Omega^T_{L_0}}\left[\prod_{u \in \Omega^T_{L_0}} \sum_{j \in \{\mathrm{L},\mathrm{N}\}} q_j(r_{u,b}) \left(1 + \frac{s}{m} P_t G_{u,b} r_{u,b}^{-\alpha_j}\right)^{-m}\right] \\ &\overset{(a)}{=} \exp\Bigg(-2\mu^T \int_0^D \Bigg[1 - \sum_{j \in \{\mathrm{L},\mathrm{N}\}} q_j(r_{b,u}) \times \\ &\qquad \left(1 + sP_v G_{b,u} r_{b,u}^{-\alpha_j}/m\right)^{-m}\Bigg] dr_{o,u}\Bigg) \\ &= \exp\left(-2\mu^T \int_0^D \Upsilon\left(sP_t G_{u,b}, r_{b,u}\right) dr_{o,u}\right), \end{aligned} \quad (68)$$

where $r_{b,u} = \sqrt{r_{o,u}^2 + r_{o,b}^2 - 2r_{o,u}r_{o,b}\cos\theta_0}$, and step (a) follows from the PGFL over a PPP.

The Laplace transform of interference from L_0 is calculated by averaging over θ_0,

$$\mathcal{L}_{I^{\mathrm{V}}_{b,0}}(s) = \int_0^\pi \frac{1}{\pi} \mathcal{L}_{I^{\mathrm{V}}_{b,0}|\theta_0}(s)\, d\theta_0. \quad (69)$$

Invoking (68) into (69) arrives at (32).

APPENDIX C
PROOF OF LEMMA 6

The Laplace transform of interference from all roads excluding the typical line is given as

$$\begin{aligned} &\mathcal{L}_{I^{\mathrm{V}}_{b,k}}(s) \\ &= \mathbb{E}_{I^{\mathrm{V}}_{b,k}}\left[\prod_{L_k \in \Phi_L} \prod_{u \in \Omega^T_{L_k}} \exp\left(-sP_t G_{u,b} |h_{u,b}|^2 r_{u,b}^{-\alpha}\right)\right] \\ &\overset{(a)}{=} \mathbb{E}_{\Phi_L}\Bigg[\prod_{L_k \in \Phi_L} \mathbb{E}_{\Omega^T_{L_k}}\Bigg[\prod_{u \in \Omega^T_{L_k}} \sum_{j \in \{\mathrm{L},\mathrm{N}\}} q_j(r_{u,b}) \times \\ &\qquad \left(1 + sm^{-1} P_t G_{u,b} r_{u,b}^{-\alpha_j}\right)^{-m}\Bigg]\Bigg] \\ &\overset{(b)}{=} \exp\Bigg(-2\pi\mu_L \int_0^D \Bigg[1 - \exp\Bigg(-2\mu^T \times \\ &\qquad \int_0^{\sqrt{D^2-\zeta_k^2}} \Upsilon\left(sP_t G_{u,b}, r\right) d\zeta_u\Bigg)\Bigg] \zeta_k d\zeta_k\Bigg), \end{aligned} \quad (70)$$

where step (a) holds as $|h_{b,u}|^2$ obeys the Gamma distribution. Using the PGFL of the PLP Phi_L and PPP $\Omega^T_{L_k}$ successively arrives at (33).

APPENDIX D
PROOF OF THEOREM 8

The SOP is defined as

$$\mathcal{P}_{so} = \mathbb{P}\left[\max_{e_i \in \Phi_e} \gamma_{o,e_i} > \beta_e\right] = 1 - \mathbb{E}_{\Phi_e}\left[\prod_{e_i \in \Phi_e} \underbrace{\mathbb{P}\left[\gamma_{o,e_i} < \beta_e\right]}_{p_{e_i}}\right]. \tag{71}$$

Clearly, the derivation of p_{e_i} is identical to that of COP given in (40), hence we can directly arrive at (59). After that, the SOP in (71) can be calculated as

$$\begin{aligned}
\mathcal{P}_{so} &= 1 - \mathbb{E}_{\Phi_L}\left[\mathbb{E}_{\Omega^E_{L_k}}\left[\prod\nolimits_{e_i \in \Omega^E_{L_k}} p_{e_i} \,|L_k \in \Phi_L\right]\right] \\
&\overset{(a)}{=} 1 - \exp\Bigg(-2\pi\mu_L \int_0^D \Bigg(1 - \\
&\qquad \mathbb{E}_{\Omega^E_{L_k}}\left[\prod\nolimits_{e_i \in \Omega^E_{L_k}} p_{e_i} \middle| L_k \in \Phi_{L_0}\right]\Bigg) d\zeta_k\Bigg) \\
&\overset{(b)}{=} 1 - \exp\Bigg(-2\pi\mu_L \int_0^D \Bigg(1 - \\
&\exp\Bigg(-2\mu^E \int_0^{\sqrt{D^2-\zeta_k^2}} (1 - p_{e_i})\, dr_{e_i}\Bigg)\Bigg) d\zeta_k\Bigg),
\end{aligned} \tag{72}$$

where step (a) follows from the PGFL over the PLP Φ_L. By further using the PGFL over the PPP $\Omega^E_{L_k}$ completes the proof.

REFERENCES

[1] P. Papadimitratos, A. D. L. Fortelle, K. Evenssen, R. Brignolo, and S. Cosenza, "Vehicular communication systems: Enabling technologies, applications, and future outlook on intelligent transportation," *IEEE Commun. Mag.*, vol. 47, no. 11, pp. 84–95, Nov. 2009.

[2] H. Hartenstein and L. P. Laberteaux, "A tutorial survey on vehicular ad hoc networks," *IEEE Commun. Mag.*, vol. 46, no. 6, pp. 164–171, Jun. 2008.

[3] S. Biswas, R. Tatchikou, and F. Dion, "Vehicle-to-vehicle wireless communication protocols for enhancing highway traffic safety," *IEEE Commun. Mag.*, vol. 44, no. 1, pp. 74–82, Jan. 2006.

[4] F. J. Martin-Vega, M. C. Aguayo-Torres, G. Gomez, J. T. Entrambasaguas, and T. Q. Duong, "Key technologies, modeling approaches, and challenges for millimeter-wave vehicular communications," *IEEE Commun. Mag.*, vol. 56, no. 10, pp. 28–35, Oct. 2018.

[5] B. M. ElHalawany, A. A. A. El-Banna, and K. Wu, "Physical-layer security and privacy for vehicle-to-everything," *IEEE Commun. Mag.*, vol. 57, no. 10, pp. 84–90, Oct. 2019.

[6] L. Liang, H. Peng, G. Y. Li, and X. Shen, "Vehicular communications: A physical layer perspective," *IEEE Trans. Veh. Technol.*, vol. 66, no. 12, pp. 10647–10659, Dec. 2017.

[7] 3GPP TR 36.885, "Study on LTE-based V2X services," Jul. 2016.

[8] S.-H. Sun, J.-L. Hu, Y. Peng, X.-M. Pan, L. Zhao, and J.-Y. Fang, "Support for vehicle-to-everything services based on LTE," *IEEE Wireless Commun.*, vol. 23, no. 3, pp. 4–8, Jun. 2016.

[9] M. Shafi, A. F. Molisch, P. J. Smith, T. Haustein, P. Zhu, P. De Silva, F. Tufvesson, A. Benjebbour, and G. Wunder, "5G: A tutorial overview of standards, trials, challenges, deployment, and practice," *IEEE J. Sel. Areas Commun.*, vol. 35, no. 6, pp. 1201–1221, Jun. 2017.

[10] J. G. Andrews, T. Bai, M. N. Kulkarni, A. Alkhateeb, A. K. Gupta, and R. W. Heath, "Modeling and analyzing millimeter wave cellular systems," *IEEE Trans. Commun.*, vol. 65, no. 1, pp. 403–430, Jan. 2017.

[11] V. Va, J. Choi, and R. W. Heath, "The impact of beamwidth on temporal channel variation in vehicular channels and its implications," *IEEE Trans. Veh. Technol.*, vol. 66, no. 6, pp. 5014–5029, Jun. 2017.

[12] W. Stallings, *Cryptography and Network Security: Principles and Practice*. Pearson Upper Saddle River, 2017.

[13] A. D. Wyner, "The wire-tap channel," *Bell Syst. Tech. J*, vol. 54, no. 8, pp. 1355–1387, Oct. 1975.

[14] C. Wang and H.-M. Wang, "Physical layer security in millimeter wave cellular networks," *IEEE Trans. Wireless Commun.*, vol. 15, no. 8, pp. 5569–5585, Aug. 2016.

[15] Y. Ju, H.-M. Wang, T.-X. Zheng, and Q. Yin, "Secure transmissions in millimeter wave systems," *IEEE Trans. Commun.*, vol. 65, no. 5, pp. 2114–2127, May 2017.

[16] Y. Ju, H.-M. Wang, T.-X. Zheng, Q. Yin, and M. H. Lee, "Safeguarding millimeter wave communications against randomly located eavesdroppers," *IEEE Trans. Wireless Commun.*, vol. 17, no. 4, pp. 2675–2688, Apr. 2018.

[17] W. Yang, L. Tao, X. Sun, R. Ma, Y. Cai, and T. Zhang, "Secure on-off transmission in mmWave systems with randomly distributed eavesdroppers," *IEEE Access*, vol. 7, pp. 32681–32692, 2019.

[18] F. Voss, C. Gloaguen, F. Fleischer, and V. Schmidt, "Distributional properties of Euclidean distances in wireless networks involving road systems," *IEEE J. Sel. Areas Commun.*, vol. 27, no. 7, pp. 1047–1055, Sep. 2009.

[19] W. Yi, Y. Liu, and A. Nallanathan, "Coverage analysis for mmWave-enabled V2X networks via stochastic geometry," *in Proc. IEEE Global Communications Conference (GLOBECOM'2019)*, Waikoloa, HI, USA, 2019, pp. 1–6.

[20] C.-S. Choi and F. Baccelli, "Poisson Cox point processes for vehicular networks," *IEEE Trans. Veh. Technol.*, vol. 67, no. 10, pp. 10160–10165, Oct. 2018.

[21] C.-S. Choi and F. Baccelli, "An analytical framework for coverage in cellular networks leveraging vehicles," *IEEE Trans. Commun.*, vol. 66, no. 10, pp. 4950–4964, Oct. 2018.

[22] V. V. Chetlur and H. S. Dhillon, "Coverage analysis of a vehicular network modeled as Cox process driven by Poisson line process," *IEEE Trans. Wireless Commun.*, vol. 17, no. 7, pp. 4401–4416, Jul. 2018.

[23] V. V. Chetlur and H. S. Dhillon, "Coverage and rate analysis of downlink cellular vehicle-to-everything (C-V2X) communication," *IEEE Trans. Wireless Commun.*, vol. 19, no. 3, pp. 1738–1753, Mar. 2020.

[24] M. N. Sial, Y. Deng, J. Ahmed, A. Nallanathan, and M. Dohler, "Stochastic geometry modeling of cellular V2X communication over shared channels," *IEEE Trans. Veh. Technol.*, vol. 68, no. 12, pp. 11873–11887, Dec. 2019.

[25] J. Choi, V. Va, N. Gonzalez-Prelcic, R. Daniels, C. R. Bhat, and R. W. Heath, "Millimeter-wave vehicular communication to support massive automotive sensing," *IEEE Commun. Mag.*, vol. 54, no. 12, pp. 160–167, Dec. 2016.

[26] M. Ozpolat, E. Kampert, P. A. Jennings, and M. D. Higgins, "A grid-based coverage analysis of urban mmWave vehicular ad hoc networks," *IEEE Commun. Lett.*, vol. 22, no. 8, pp. 1692–1695, Aug. 2018.

[27] Z. Zhang, L. Wang, Z. Bai, K. S. Kwak, Y. Zhong, X. Ge, and T. Han, "The analysis of coverage and capacity in mmWave VANET," *in Proc. 10th International Conference on Communication Software and Networks (ICCSN'2018)*, Chengdu, China, 2018, pp. 221–226.

[28] Y. Wang, K. Venugopal, A. F. Molisch, and R. W. Heath, "MmWave vehicle-to-infrastructure communication: Analysis of urban microcellular networks," *IEEE Trans. Veh. Technol.*, vol. 67, no. 8, pp. 7086–7100, Aug. 2018.

[29] W. Yi, Y. Liu, Y. Deng, A. Nallanathan, and R. W. Heath, "Modeling and analysis of mmWave V2X networks with vehicular platoon systems," *IEEE J. Sel. Areas Commun.*, vol. 37, no. 12, pp. 2851–2866, Dec. 2019.

[30] N.-Y. Ahn, D.-H. Lee, and S.-J. Oh, "Vehicle communication using secrecy capacity," *in Proc. Future Technologies Conference*. Springer, Cham, 2018.

[31] Y. Ai, M. Cheffena, A. Mathur, and H.-J. Lei, "On physical layer security of double rayleigh fading channels for vehicular communications," *IEEE Wireless Commun. Lett.*, vol. 7, no. 6, pp. 1038–1041, Jul. 2018.

[32] C. Wang, Z. Li, J. Shi, J. Si, and D. W. K. Ng, "Physical layer security of vehicular networks: A stochastic geometry approach," *in Proc. IEEE International Conference on Communications (ICC'2020)*, Dublin, Ireland, 2020, pp. 1–7.

[33] C. Wang, Z. Li, X.-G. Xia, J. Shi, J. Si, and Y. Zou, "Physical layer security enhancement using artificial noise in cellular vehicle-to-everything (C-V2X) networks," *IEEE Trans. Veh. Technol.*, vo. 69, no. 12, pp. 15253–15268, Dec. 2020.

[34] M. E. Eltayeb, J. Choi, T. Y. Al-Naffouri, and R. W. Heath, "Enhancing secrecy with multiantenna transmission in millimeter wave vehicular communication systems," *IEEE Trans. Veh. Technol.*, vol. 66, no. 9, pp. 8139–8151, Sep. 2017.

[35] S. Vuppala, Y. J. Tolossa, G. Kaddoum, and G. Abreu, "On the physical layer security analysis of hybrid millimeter wave networks," *IEEE Trans. Commun.*, vol. 66, no. 3, pp. 1139–1152, Mar. 2018.

[36] T.-X. Zheng, H.-W. Liu, N. Zhang, Z. Ding, and V. C. M. Leung, "Secure content delivery in two-tier cache-enabled mmWave heterogeneous networks," *IEEE Trans. Inf. Forensics Security*, vol. 16, pp. 1640–1654, 2021.
[37] A. Thornburg, T. Bai, and R. W. Heath, "Performance analysis of outdoor mmWave ad hoc networks," *IEEE Trans. Signal Process.*, vol. 64, no. 15, pp. 4065–4079, Aug. 2016.
[38] S. N. Chiu, D. Stoyan, W. S. Kendall, and J. Mecke, *Stochastic Geometry and Its Applications*. New York, NY, USA: Wiley, 2013.
[39] M. Haenggi, *Stochastic Geometry for Wireless Networks*. Cambridge University Press, 2012.
[40] I. S. Gradshteyn, I. M. Ryzhik, A. Jeffrey, D. Zwillinger, and S. Technica, *Table of Integrals, Series, and Products*, 7th ed. New York: Academic Press, 2007.

Tong-Xing Zheng (Member, IEEE) received the B.S. degree in information engineering and Ph.D. degree in information and communications engineering from Xi'an Jiaotong University, Xi'an, China, in 2010 and 2016, respectively. From 2017 to 2018, he was a Visiting Scholar with the School of Electrical Engineering and Telecommunications, University of New South Wales, Sydney, Australia. He is currently an Associate Professor with Xi'an Jiaotong University. His current research interests include 5G&6G wireless networks and key technologies, physical layer security, and covert communications. He has co-authored the book *Physical Layer Security in Random Cellular Networks* (Springer, 2016), one book chapter, and has authored or co-authored over 70 papers in telecommunications journals and conference proceedings. He was a recipient of the Excellent Doctoral Dissertation Award of Shaanxi Province in 2019 and the First Prize of Science and Technology Award in Higher Institution of Shaanxi Province in 2019. He was honored as an Exemplary Reviewer of IEEE TRANSACTIONS ON COMMUNICATIONS in 2017, 2018, and 2021, respectively. He was a Leading Guest Editor of FRONTIERS IN COMMUNICATIONS AND NETWORKS for the Special Issue on Covert Communications for Next-Generation Wireless Networks in 2021 and a Guest Editor of WIRELESS COMMUNICATIONS AND MOBILE COMPUTING for the Special Issue on Physical Layer Security for Internet of Things in 2018. He is currently serving as an Associate Editor of IET ELECTRONIC LETTERS and a Review Editor of FRONTIERS IN COMMUNICATIONS AND NETWORKS.

Yating Wen received the B.S. degree in electronic information engineering from Chang'an University, Xi'an, China, in 2019, and the M.S. degree in information and communications engineering from Xi'an Jiaotong University, Xi'an, China, in 2022. Her research interests include physical-layer security and mobile edge computing.

Hao-Wen Liu received the B.S. degree in information science and technology from Southwest Jiaotong University, Chengdu, China, in 2017, and the M.S. degree in cyber science and engineering from Xi'an Jiaotong University, Xi'an, China, in 2021. His research interests include physical-layer security of mmWave networks, cache-enabled networks, and cellular vehicle-to-everything networks.

Ying Ju (Member, IEEE) received the B.S. and M.S. degrees in electronic information engineering from Tianjin University, Tianjin, China, in 2008 and 2010, respectively, and the Ph.D. degree in information and communications engineering from Xi'an Jiaotong University, Xi'an, China, in 2018. From 2016 to 2017, she was a Visiting Scholar with the Department of Computer Science, University of California, Santa Barbara, USA. From 2010 to 2018, she was a Senior Engineer with the State Radio Monitoring Center, Xi'an, China. She is currently an Associate Professor with the Department of Telecommunications Engineering, Xidian University, Xi'an, China. Her research interests include physical layer security of wireless communications, millimeter wave communication systems, and stochastic geometry.

Hui-Ming Wang (Senior Member, IEEE) received the B.S. and Ph.D. degrees in electrical engineering from Xi'an Jiaotong University, Xi'an, China, in 2004 and 2010, respectively. From 2007 to 2008 and from 2009 to 2010, he was a Visiting Scholar with the Department of Electrical and Computer Engineering, University of Delaware, USA. He is currently a Full Professor with Xian Jiaotong University. His research interests include 5G communications and networks, intelligent communications, physical-layer security, and covert communications. He has coauthored the book *Physical Layer Security in Random Cellular Networks* (Springer, 2016) and authored or coauthored over 150 IEEE journals and conference papers. He was the Clarivate Highly Cited Researcher in 2019 and Elsevier Highly Cited Researcher in 2020. He received the IEEE ComSoc Asia-Pacific Best Young Researcher Award in 2018, the National Excellent Doctoral Dissertation Award in China in 2012, and the Best Paper Award from the IEEE/CIC International Conference on Communications, China, in 2014. He is currently an Associate Editor of the IEEE TRANSACTIONS ON COMMUNICATIONS.

Kai-Kit Wong (Fellow, IEEE) received the BEng, the MPhil, and the PhD degrees, all in Electrical and Electronic Engineering, from the Hong Kong University of Science and Technology, Hong Kong, in 1996, 1998, and 2001, respectively. After graduation, he took up academic and research positions at the University of Hong Kong, Lucent Technologies, Bell-Labs, Holmdel, the Smart Antennas Research Group of Stanford University, and the University of Hull, UK. He is Chair in Wireless Communications at the Department of Electronic and Electrical Engineering, University College London, UK. His current research centers around 5G and beyond mobile communications. He is a co-recipient of the 2013 IEEE Signal Processing Letters Best Paper Award and the 2000 IEEE VTS Japan Chapter Award at the IEEE Vehicular Technology Conference in Japan in 2000, and a few other international best paper awards. He is Fellow of IEEE and IET and is also on the editorial board of several international journals. He is the Editor-in-Chief for IEEE WIRELESS COMMUNICATIONS LETTERS since 2020.

Jinhong Yuan (Fellow, IEEE) received the B.E. and Ph.D. degrees in electronics engineering from the Beijing Institute of Technology, Beijing, China, in 1991 and 1997, respectively. From 1997 to 1999, he was a Research Fellow with the School of Electrical Engineering, The University of Sydney, Sydney, Australia. In 2000, he joined the School of Electrical Engineering and Telecommunications, The University of New South Wales, Sydney, Australia, where he is currently a Professor and the Head of Telecommunication Group with the School. He has published two books, six book chapters, over 300 papers in telecommunications journals and conference proceedings, and 50 industrial reports. He is a co-inventor of one patent on MIMO systems and two patents on low-density-parity-check codes. His current research interests include error control coding and information theory, communication theory, and wireless communications. He has co-authored four Best Paper Awards and one Best Poster Award, including the Best Paper Award from the IEEE International Conference on Communications, Kansas City, USA, in 2018, the Best Paper Award from IEEE Wireless Communications and Networking Conference, Cancun, Mexico, in 2011, and the Best Paper Award from the IEEE International Symposium on Wireless Communications Systems, Trondheim, Norway, in 2007. He served as the IEEE NSW Chapter Chair of Joint Communications/Signal Processions/Ocean Engineering Chapter during 2011–2014. He has served as an Associate Editor for the IEEE TRANSACTIONS ON COMMUNICATIONS during 2012–2017. He is currently serving as an Associate Editor for the IEEE TRANSACTIONS ON WIRELESS COMMUNICATIONS.